Investigating the controls on fault rock distribution in normal faulted shallow burial limestones, Malta, and the implications for fluid flow

Authors:

Andy P. Cooke[a] *, Quentin J. Fisher[a], Emma A.H. Michie[b], Graham Yielding[b]

a: School of Earth and Environment, University of Leeds, Leeds, LS2 9JT, United Kingdom

b: Badley Geoscience Limited, North Beck House, North Beck Lane, Hundleby, Spilsby, Lincolnshire, PE23 5NB, United Kingdom

E-mail address: eeapc@leeds.ac.uk (A.P. Cooke); q.j.fisher@leeds.ac.uk (Q.J. Fisher); emma@badleys.co.uk (E.A.H. Michie); graham@badleys.co.uk (G. Yielding).

Corresponding author. Tel.: +44(0) 7557 795 278

Keywords:

Faulting; Fault rock; Fault zone architecture; Carbonate; Fault seal; Cataclasite

Abstract

The spatial distribution and fabric of carbonate fault rocks observed at outcrop are often highly heterogeneous. Therefore, petrophysical properties of fault rock samples may not be representative of the overall sealing capacity of the fault zone. By quantifying the fault rock distributions (i.e. fault rock thickness and fault rock continuity) of several fault zones in Malta, juxtaposing shallow burial limestones, this work investigates the relationship between fault zone architecture, deformation mechanisms, and fault rock distribution. Results from microstructural analyses indicate that high porosity (>15 %) grain-dominated limestones deform via grain scale deformation, as opposed to fracture-derived cataclasites often observed in tight carbonates. Low porosity (<15 %) grain-dominated limestones and high porosity micrite-dominated limestones deform in a more distributed manner, through extensional fracturing and brecciation. Fault rock continuity estimates suggest displacements of 50-200 m are required to form a continuous low-permeability cataclasite veneer in the studied sequence. However, greater displacements may be required when a distributed damage zone is present, in which strain is accommodated over multiple slip surfaces. This work highlights the heterogeneity in the distribution and fabric of carbonate fault rocks within fault zones hosting tens of meters displacement, and the importance of considering fault rock thickness and continuity when estimating the sealing capacity of a carbonate-hosted fault zone.

1. Introduction

Faults have been documented to impact fluid flow in the subsurface, (Smith, 1980; Taylor and Dietvorst, 1991; Knai and Knipe, 1998; Wiprut and Zoback, 2000; Fisher and Knipe, 2001; Jolley et al., 2007). Although there are documented examples of carbonate-hosted fault zones acting as barriers to fluid flow (e.g. Bockel-Rebelle et al., 2004; Birkle and Angulo, 2005; Vega Riveros et al., 2011; Corona et al., 2012), their impact on flow is poorly understood, despite the global importance of carbonate reservoirs in hydrocarbon reserves; around 60% of global oil reserves and 40% of global gas reserves are stored in carbonates (Schlumberger, 2007). Past research into the sealing potential of faults has been primarily directed towards siliciclastic hydrocarbon reservoirs (e.g. Knipe 1992; Antonellini & Aydin 1994; Caine et al. 1996; Evans et al. 1997; Fulljames et al. 1997; Yielding et al. 1997; Fisher & Knipe 2001; Crawford et al. 2002; Flodin et al. 2005; Færseth et al. 2007). These studies indicate that fault zone structure can provide useful insights into the potential for across-fault fluid flow within the subsurface (Caine et al., 1996; Evans et al., 1997; Rawling et al., 2001).

Fault rock distributions and observed deformation mechanisms are controlled by a number of factors, including fault zone architecture and host rock properties (Mitchell and Faulkner, 2009; Michie et al., 2014). Fault zone studies in both siliciclastic and crystalline rocks have enabled the development of a conceptual model for fault zone architecture. Slip along a fault commonly produces a localised fault core, or several strands of fault core, surrounded by a damage zone in which damage decreases exponentially into the undeformed protolith (Aydin and Johnson, 1978; Chester and Logan, 1986; Caine et al., 1996; Shipton and Cowie, 2001; Kim et al., 2004; Mitchell and Faulkner, 2009; Riley et al., 2010). In general, the fault core is composed of high strain products that destroy the protolith fabric and are often characterised by a low permeability that may act as barriers or baffles to flow. The surrounding damage zone, typically containing a high fracture density whilst mostly preserving the protolith fabric, is commonly considered a conduit to flow (e.g. Chester & Logan 1986; Chester et al. 1993; Antonellini & Aydin 1994; Wibberley & Shimamoto 2003; Mitchell & Faulkner 2009). However, depending on the porosity, texture and stress conditions at the time of faulting, the damage zone may act as a barrier to flow, particularly in clastic reservoirs (Fossen et al., 2007).

This fault zone model has been shown to also be broadly applicable to carbonate-hosted fault zones (Agosta and Kirschner, 2003; Storti et al., 2003; Micarelli et al., 2006); continuous low permeability fault cores, likely to act as a barrier or partial barrier to flow, and fractured damage zones, likely to have enhanced permeability, are documented in carbonate rocks (e.g. Micarelli et al. 2006; Agosta et al. 2007; Agosta 2008). However, carbonate-hosted fault zones are commonly documented to have a variety of additional structural elements. These include fault cores consisting of discontinuous lenses of fault rock exhibiting a variety of fabrics and petrophysical properties (e.g. Michie & Haines 2016), fault zones with permeable deformation products, such as fracturing and fault breccia, likely to allow up- and along-fault fluid flow (e.g. Lee et al. 1997; Matonti et al. 2012), and fault zones that host a fracture splay zone, whereby fractures and subsidiary slip surfaces are generated at a point of strain accumulation, relating to the mechanical stratigraphy imposed by juxtaposing two lithofacies with contrasting mechanical properties (Michie et al., 2014). The variable architectures associated with these examples control the distribution of fault rock and, ultimately, the fluid flow throughout the fault zone. Therefore, it is important to consider how these architectures are generated with respect to the host rock and fault kinematics.

Understanding fault rock distributions requires quantifiable physical parameters, such as fault rock thickness (FRT) and fault rock continuity (FRC). Empirical relationships between fault displacement and FRT, recorded from a combination of field and subsurface core studies, enables the prediction of FRT for any fault of known displacement (Hull, 1988; Wibberley et al., 2008; Childs et al., 2009; Solum and Huisman, 2017). This data is directly applicable to the estimation of fault sealing potential over production timescales through the use of transmissibility multipliers (Manzocchi et al., 1999). However, empirical data varies over several orders of magnitude for any given displacement (e.g. Hull 1988) due to the architectural heterogeneity between fault zones. This method of thickness estimation also assumes a continuous fault core, which is often not observed at outcrop (e.g. Micarelli et al. 2006; Joussineau & Aydin 2007; Bauer et al. 2016).

Several studies consider the continuity of shale smear within siliciclastic hosted fault zones (e.g. Yielding et al. 1997; Færseth 2006). However, there is limited research into the spatial heterogeneity of fault rock distributions in carbonate rocks (e.g. Bonson et al., 2007). Studies of high porosity carbonate-hosted fault zones have suggested that fault rock becomes continuous after 5 m displacement based upon thickness measurements along vertically exposed fault zone cross sections (Micarelli et al., 2006). Studies of low porosity carbonate-hosted fault zones have suggested that cataclastic fault rocks only become continuous at high displacements. However, portions of impermeable cataclasite are not considered continuous enough to have a regional impact on flow (Bauer et al., 2016). Studies of fault zones in Malta have suggested that fault cores are continuous at displacements greater than 30 m, due to fault rock being distributed across multiple slip surfaces generated within weaker layers (Michie and Haines, 2016). Despite the importance of a continuous fault core, to the authors' knowledge, no quantified carbonate-hosted FRC measurements have previously been published.

This research aims to improve the understanding of fault rock distribution in shallow water limestones by investigating the architectural controls on fault rock formation and by providing a quantified study of FRT and FRC in faulted Oligo-Miocene limestones. Accordingly, this study presents results from the analysis of 3 fault zones outcropping in eastern Gozo, Malta, from which fault zone mapping and outcrop structural data are used to interpret the fault zone architecture and the distributions of fault rock. The deformation mechanisms observed within each fault zone are characterised using microstructural analysis, thereby providing an understanding of the architectural and lithological controls on fault rock fabric. FRT measurements and FRC estimates are presented from 6 Maltese fault zones, investigating the control of fault displacement, host rock lithofacies, and fault zone architecture on fault rock distribution. This study highlights the importance of considering FRT heterogeneity and FRC within carbonate-hosted fault zones when estimating their hydraulic behaviour.

1.1. Geological setting

Field analysis was undertaken from 6 fault zones within the islands of Malta (Figure 1C). Detailed fault zone architecture and microstructural investigations were undertaken for 3 of these fault zones located on the eastern tip of the island of Gozo (Figure 1C, Faults A-C). Malta is characterised by well exposed, faulted Oligo-Miocene reef limestones with limited post deformation diagenesis. The studied faults offset the simple sequence with displacements ranging from several meters to hundreds of meters. Faulted outcrops often enable a study of faulting in either, or both, cross sectional and map views due to the morphology of the islands, which includes raised beaches, limited vegetation, and prominent cliffs. Fault surfaces often form cliff faces themselves, such as the Il Maghlaq Fault (IMF) (Figure 1B & C), due to a resistance to weathering or the poor preservation of the hanging wall damage zone, allowing along strike fault rock measurements to be undertaken.

‘figure 1 here’

1.2. Tectonic framework

The Maltese Islands (Malta, Comino, and Gozo) are located on the northern flank of the Pantelleria rift (Illies 1981; Boccaletti et al. 1987, Figure 1A). The Pantelleria rift comprises a series of elongated, fault controlled rift basins of Miocene-Pliocene age situated at the centre of the Pelagian block (Reuther and Eisbacher, 1985), a shelf bridge connecting the Hyblean Plateau of Southern Sicily and the Tripolitanian platform of northern Libya. Rifting began simultaneously with mountain belt formation in the Oligocene, forming a complex sequence of horst and grabens, including the Maltese graben system which dominates the faulting in Malta (Reuther & Eisbacher 1985; Jongsma et al. 1987; Dart et al. 1993, Figure 1B). There are 2 intersecting fault trends within this system, ENE-WSW and WNW-ESE, resulting from N-S extension (Pedley et al. 1976; Reuther & Eisbacher 1985; Dart et al. 1993, Figure 1B). The dominant onshore fault trends (ENE-WSW) are related to the North Malta Graben, which is bound by 2 major normal faults: the Victoria Lines Fault (VLF) and the South Gozo

Fault (SGF) which crosscut Malta and outcrop along the south coast of Gozo, respectively (Figure 1C).

Gozo, located to the North of Malta, has a gentle regional dip to the NE and is dominated by normal faults roughly parallel to the SGF (Pedley et al., 1976). A series of narrow, asymmetric graben or tilt blocks extend inland from the SGF at an angle of c. 50° (Figure 2A), interpreted as en echelon structures relative to the dextral shear pattern of the SGF (Illies, 1981). This series of faults includes 2 of the studied fault zones, namely the Qala Point Fault Zone (QPFZ) and the South Qala Fault (SQF) (Figure 2B).

'figure 2 here'

1.3. Stratigraphic framework

Carbonate lithofacies has previously been shown to exert some control on the deformation microstructures; micrite-dominated rocks (mudstones – wackestones) typically deform in a distributed manner, whereas grain-dominated rocks (packstone – grainstones) deform in a more localised manner on the grain scale (Michie et al., 2014). Therefore, the dominant lithofacies of each formation is noted for simplification.

The Maltese sequence consists of a simple 'layer cake' succession of Oligocene – Miocene, shallow burial carbonates (Figure 1D). The oldest exposed units consist of a series of shallow water reef limestones (Lower Coralline Limestone, Figure 3), succeeded by pelagic foraminiferal wackestones (Globigerina Limestone, Figure 3), a carbonate rich clay layer (Blue Clay), and finally additional reef limestone successions (Upper Coralline Limestone, Figure 3).

1.3.1. Lower Coralline Limestone (grain-dominated)

The base of the exposed succession on Malta is formed by the Chattian (Oligocene) Lower Coralline Limestones (LCL) (Figure 1D &Figure 3). The LCL is primarily composed of grainstones and packstones. A maximum of 140 m of LCL is exposed onshore, despite its thickness reaching up to 1000 m offshore (Pedley et al., 1976; Bonson et al., 2007). The LCL varies from pale yellow biomicrites at its base, to massively bedded coralline algal limestones, and finally coarse bioclastic limestones displaying cross bedding at the top (Pedley et al., 1976; Pedley, 1978; Brandano et al., 2009). Pedley (1978) divided the LCL into 4 members that are non-uniformly distributed across the islands, these are (oldest to youngest): the Maghlaq Member, the Attard Member, the Xlendi Member and the Il-Mara Member. The Attard and Xlendi members are the only members present within the principal study areas, therefore are the only members discussed:

- The Attard member is a rhodolitic algal packstone containing coral, red algae and larger benthonic formanifera, deposited on the inner and middle ramp (Pedley 1978; Brandano et al. 2009, Figure 3). The Attard member has a porosity of 10 – 15%.
- The Xlendi member is a succession of bioclastic packstone units, including the Scutella beds, displaying upwards shallowing and cross bedded biosparites (Figure 3). Depositional setting is interpreted as a shoal environment (Pedley, 1978; Brandano et al., 2009). It often occurs laterally to and above the Attard member. The Xlendi member has a porosity of 25 – 30%.

1.3.2. Globigerina Limestone (micrite-dominated)

The LCL is capped by a hardground, which in turn is overlain by the Globigerina Limestone Member (GL) pelagic carbonates of Aquitanian to Serravallian age (Pedley et al.

1976; Dart et al. 1993, Figure 1D). The GL is a succession of fine-grained biomicritic wackestones and marls containing primarily planktonic foraminifera (*Globigerina*) (Figure 3), representing a deepening to an outer shelf environment (Pedley, 1978; Bonson et al., 2007). Two hardgrounds, overlain by phosphoritic conglomeratic layers (<0.7 m in thickness), separate the formation into the Lower, Middle and Upper Globigerina Limestone members (LGL, MGL and UGL respectively) (Pedley 1978; Pedley & Bennett 1985; Bonson et al. 2007; Figure 3). The LGL consists of pale cream to yellow packstones becoming wackestones just above the base and are cut by neptunian dykes, hence marking the onset of rifting (Dart et al., 1993). The MGL is a sequence of massive white carbonate mudstones and marls. The UGL comprises cream wackestones with a central pale grey marl. The thickness of the GL formation varies from 40 – 75 m (Pedley et al., 1976; Dart et al., 1993). However, the MGL and C2 thin southward across Gozo until they become absent, resuming in northern Malta (Figure 1D). The GL has a porosity of 30 – 36%.

1.3.3. Blue Clay (clay)

The Blue Clay formation (mid to late Serravalian) consists of light and dark grey banded marls, in which lighter colours contain greater proportion of carbonate. The Blue Clay is rich in kaolinite, glauconite, and contains up to 30% carbonate with a *c.*75 % phyllosilicate content (John et al., 2003). Formation thickness varies from a maximum of 65 m to areas of absence (rift margins in eastern Malta) (Pedley et al., 1976; Dart et al., 1993).

1.3.4. Upper Coralline Limestone (micrite/grain-dominated)

The youngest outcropping unit within the Maltese sequence is the Upper Coralline Limestone (UCL), of Late Tortonian to Messinian age (Bosence & Pedley 1982; Bonson et al. 2007, Figure 1D). The lowermost part of the UCL consists of coralline algal biostrome facies, known as the Mtarfa member, moving upward into a coral and algal patch reef facies, known as the Tal-Piktal member (Bosence and Pedley, 1982; Dart et al., 1993). The upper part of the UCL is characterized by significant fault controlled facies distributions, areas of non-deposition, and major growth faults characterized by divergent fanning strata (Dart et al., 1993). The 2 members present within the study zone are the Mtarfa member, containing thickly bedded mudstones and wackestones, and the Tal-Piktal member, a pale grey wackestone to packstone (Figures 1D and 3). Both members have porosities in the range of 25 – 35%.

'figure 3 here'

2. Methodology

2.1. Sample collection

Oriented hand specimen sized samples were collected for microstructural and petrophysical property analysis. Sample collection aimed to represent any heterogeneity present within the fault zone whilst collecting undeformed host samples for comparison.

2.2. Fault zone mapping

Georeferenced orthomosaic maps were created to enable accurate fault zone mapping. To produce the maps, georeferenced aerial photos were taken with a DJI Phantom 3 Professional drone along automated flight paths. Flight elevation was selected based upon the resolution required at each outcrop; elevations ranged from 10-50 m for high and low resolution requirements, respectively. The front and side image overlap was >65 % to ensure successful photo stitching. Maps were combined with structural field data to produce accurate geological maps of each locality.

Fault rock thickness (FRT) measurements were taken along fault strike at regular intervals (0.5-1 m) for each fault zone with accessible exposure. Thickness measurements were differentiated according to fault rock fabric, allowing for the thickness of each fault rock fabric to be compared. Fault rock continuity (FRC) was estimated as a ratio of total fault rock length to the total exposed length of the fault segment. Cataclasite FRT measurements and FRC estimates were taken at all fault zones highlighted in Figure 1. However, only 3 fault zones are suitable for along strike FRT measurements and FRC estimates for the entire fault zone width (i.e. well exposed and accessible fault zones, thereby allowing FRT measurements), namely the QPFZ (30 m displacement), the Ras il-Bajjada (RiB) fault strand of the Il-Maghlaq fault (IMF) (50 m displacement), and the Victoria Lines Fault (VLF) at Madliena Tower (90 m displacement).

2.3. Scan Lines

Circular window scan lines were used to determine the intensity of planar features (i.e. fractures and deformation bands) (Mauldon and Dershowitz, 2000; Mauldon et al., 2001; Rohrbaugh et al., 2002). Circular scan lines are best suited to avoid sampling bias relating to orientation of fracture traces. Scan lines were applied along transects perpendicular and parallel to principal slip surfaces at different spacing along strike to capture variation in such parameters. One transect was used to measure fracture intensities across the QPFZ and three scan lines were used to measure deformation band intensities in the accessible portion of the SGF hanging wall.

2.4. Microstructural analysis

Resin-impregnated polished thin sections were analysed using an optical microscope and a CAMSCAN CS44 scanning electron microscope. Fault rock samples were oriented in planes parallel and perpendicular to fault dip, whereas host rock samples were oriented relative to bedding. Samples were impregnated with low viscosity resin containing a blue dye to make pore spaces more apparent. Where core plugs could not be obtained, image analysis of BSE-SEM images was undertaken to estimate the sample porosity. Image analysis was also used to measure grain orientations within deformation bands. To do so, the long axis of grains was superimposed to the image and the grain Feret angles were calculated (orientation of grain Feret diameter).

2.5. Porosimetry

To measure host porosity, 1.5 inch core plugs were drilled from the collected samples. Core plugs were cleaned to remove salts using deionised water saturated with carbonate sediment of the same composition as the sample. Once clean, core plugs were dried at 60° for >4 days. The bulk volume of the core plugs was calculated using calipers to measure core plug length and diameter, with a precision of 0.01 mm. Sample grain volumes were then calculated according to Boyle’s Law using a double cell helium porosimeter. Porosity was calculated using the calculated grain and bulk volumes.

3. Results

3.1. Fault zone architecture

3.1.1. South Gozo Fault (SGF)

The SGF is a 65° SE dipping normal fault, juxtaposing the Tal-Piktal member of the UCL (hanging wall) against the top of the Blue Clay and base of the UCL Mtarfa member (footwall) (Figure 4D). Based upon the thickness of the Mtarfa and Tal-Piktal members, 16 m and >25 m respectively, fault displacement is at least 25 m. The SGF at Qala Point intersects and terminates against the SQF (Figure 2B), however there is no obvious preserved interaction between these 2 intersecting fault traces. A second slip surface, parallel to the SQF, is interpreted within the coastal inlet, between which the Blue Clay formation is entrained in a clay smear (Figure 2B). The smearing of the Blue Clay formation is common throughout all Maltese fault zones with similar stratigraphic juxtapositions (i.e. where the Blue Clay is visibly offset).

The hanging wall and the footwall both contain intense deformation band arrays surrounding the SGF. Deformation bands appear as light ridges on the weathered surface as they are more resistant to weathering than the host rock. Figure 4 shows their dominant trends (*c.*030-060° dominant trend and *c.*150-170° conjugate trend), which reflect the trend of the SGF. Scan line measurements taken >2 m from the principal slip surface show that hanging wall deformation band density and intensity do not appear to correlate with distance from the principal slip surface over the scale that scan lines were undertaken (average intensity is *c.*11 m^{-1} and average density is *c.*21 m^{-2}). However, closer to the principal slip surface (<2 m), intensities observed from hand specimens and core plugs drilled perpendicular to faulting show intensity increasing rapidly towards the principal slip surface within both the hanging wall and footwall (Figure 4E). Although no footwall scan lines were undertaken, footwall hand specimen samples at *c.*5 m from the principal slip surface show deformation band intensities that correlate with the scan line and core plug data recorded in the hanging wall.

The hanging wall principal slip surface contains a cataclasite veneer which is pale brown or grey in colour, cohesive, contains some fracturing, and <30 cm thick. In addition to the anastomosing deformation band array, the footwall consists of a region of intensely fractured wall rock up to 1 m thick. The intense fracturing has brecciated the wall rock into angular fragments ranging from 1 cm to 10 cm in size. These fragments do not appear to reduce in size towards the principal slip surface.

'figure 4 here'

3.1.2. South Qala Fault (SQF)

The South Qala Fault is a normal fault with 2 well exposed slip surfaces, striking WNW-ESE, dipping *c.*61° SSW, with a minimum of 50 m displacement (Figure 5). The footwall stratigraphy at outcrop consists of the LCL Xlendi member, LGL, UGL, and the Blue Clay. The hanging wall consists of the Blue Clay formation. However, there is no preserved hanging wall damage zone, thus the entire damage zone width cannot be determined. The 2 fault traces form a right stepping relay zone, with a bridge fault in between (Figure 5A). The exposed LGL beds forming a relay ramp (Figure 5D) are immediately adjacent to the Blue Clay formation, such that the UGL is absent. This geometry suggests the relay has become breached, with

>30 m on the breaching fault itself which is not clearly exposed. The lowermost LGL beds within the relay ramp have an increased fracture intensity and have increasing dip towards the southern fault strand (Figure 5D). These beds eventually become fault parallel and entrained within the fault zone, at which point they exhibit intense microfracturing and brecciation to form a lens of preserved GL fault rock, elongated in the direction of dip.

The western fault trace is entirely composed of a polished, micrite-dominated, GL slip surface, with rake varying from 80-90° SW (Figure 5B). The micrite-dominated slip surface is populated by a number of fault splays, parallel slip surfaces, and lenses of intensely fractured and brecciated GL (Figure 5E). There is >1 slip surface along the majority of the fault strand length; a subsidiary slip surface runs parallel to the principal slip surface along the entire fault length, <5 cm into the footwall. The GL is recrystallized or cemented between these slip surfaces in certain areas, behind which fault parallel fractures extend into the footwall. At regions of fault corrugations and when the fault strand is right-stepping, additional slip surfaces are present with 0.1 – 1 m separation. Whilst the GL in the footwall damage zone has an increased fracture intensity, the matrix remains intact. Fractures are open with no fracture cements.

Breccia clasts are rounded to subrounded within the fault core with a matrix composed of disaggregated GL. Intact clasts are composed of fractured GL and range in diameter from small cm scale clasts up to 20 – 30 cm blocks. These discrete fault breccia lenses often contain multiple localised coalescing slip surfaces displaying slickensides in a variety of directions, including strike slip or low angle (< 20°) normal slip movement. The locations of breccia lenses correlate with regions where the fault is undulating or right stepping.

The SE fault segment is composed of a polished, grain-dominated, Xlendi slip surface with vertical slickensides (Figure 5C). Several breccia lenses can be seen along the Xlendi slip surface, though their composition is unknown due to inaccessibility. The lateral tips of the lenses correspond to splays from the slip surface, creating multiple subsidiary slip surfaces through the lens. However, these lenses are generally thinner and occur less frequently along fault strike than the GL fault breccia lenses. Unlike the NW fault segment, the SE segment does not appear to be as right stepping in its geometry.

'figure 5 here'

3.1.3. Qala Point Fault Zone (QPFZ)

The Qala point fault zone (QPFZ) is the northernmost en echelon shear structure of the SGF (Figure 2). The QPFZ is a south dipping high angle (> 80°) dextral oblique normal fault zone with *c.*30 m normal displacement, and an undetermined strike slip component, distributed over several slip surfaces. At outcrop, the principal slip surface juxtaposes the Xlendi member of the LCL (hanging wall) against the Attard member of the LCL (footwall). Both members are grain-dominated carbonates, however mechanical properties may vary due to the reduced porosity of the Attard member relative to the Xlendi member (φ = *c.*10-15 % and 25-30 %, respectively). A complex zone of fracturing and subsidiary slip surfaces extends to the north of the principal slip surface, with numerous additional fault strands that appear to host offset (Figure 6). However, individual fault strand displacements cannot be determined due to the lack of marker beds and the strike slip component to slip. Several right-stepping pull-apart structures are present within the fault zone (Figure 6 & Figure 12), in agreement with the dextral oblique faulting trend of the SGF shear structure (Figure 2A). The pull-apart structures contain cross cutting Riedel shear slip surfaces of small offset and an increased fracture intensity. Larger scale Riedel shear fractures can be interpreted across the entire fault zone exposure.

Fracture intensity measurements along a transect oriented perpendicular to faulting (Figure 6) record fracture intensity increasing from a background level of < 5 m^{-1} up to >15 m^{-1} within the fault zone. The largest fracture intensities correlate to a region of several meters surrounding the principal slip surface, and to 5 m into the footwall. These fractures are often filled with an orange-brown cemented core that other fractures often terminate against.

Fault displacement is distributed across the entire zone, leading to a wide, discontinuous fault rock distribution. Fault breccia and cemented fault cores dominate fault rock fabrics within the QPFZ. Fault breccia occurs as discrete lenses bound by fault splays, and within dextral pull apart structures. Breccia lenses exhibit sharp contacts with the protolith.

‘figure 6 here’

3.2. Fault rock microstructures

3.2.1. South Gozo Fault (SGF)

The footwall and hanging wall (Mtarfa and Tal-Piktal members of the UCL) both show similar deformation and diagenetic microstructures. However, at outcrop, well developed cataclasite is limited to a veneer along the hanging wall (Figure 7). Hand specimens show there to be a sharp contact between host rock and cataclastic rock (Figure 7A), best developed where the cataclasite is thickest. BSE-SEM images show the cataclasite to have a low porosity, with pore sizes in the microporosity range (<30 µm) and the sharp contact showing a contrast between medium and low porosity rock (Figure 7B). Grain size within the cataclasite is reduced relative to the host rock; however, remnant 'survivor' bioclasts that have not been subject to cataclasis are distributed throughout the fine grained matrix. Minor pressure solution seams and sutured grain boundaries around individual fossil clasts are present within the cataclasite rock (Figure 7C & D). Remnant bioclasts within the cataclasite have been subject to aggrading neomorphism in the areas of highest deformation, formed of sparry calcite cement (Figure 7D). Survivor bioclasts are predominantly echinoderms, benthic foraminifera, and planktonic foraminifera, whereas other skeletal fossils present within the host rock appear to have been subject to preferential deformation through pore collapse and comminution.

The deformation bands present throughout the fault zone contain intact fossil clasts that have undergone little grain comminution or fracturing (cataclasis). However, the fine grained matrix between these grains indicates preferential cataclasis of the weakest grains has occurred. Quantitative image analysis of grain orientations (grain Feret diameter orientations) shows alignment of grains from bedding orientations to deformation band parallel (Figure 8). BSE-SEM imagery shows a reduction in porosity from *c.*20-25 % down to *c.*5-10 % from the host sediment surrounding deformation bands to the sediment within the deformation bands (Figure 8B).

Intergranular microspar cements are present within the host rock but are not pore filling, maintaining good intergranular porosity and pore connectivity. However, these cements occlude remnant porosity in the cataclasite and deformation bands, such that the primary porosity consists of intragranular pore spaces within fossil structures and microporosity between microspar crystals. Overall, pore connectivity appears far lower in the fault rock than within the host rock.

‘figure 7 here’

‘figure 8 here’

3.2.2. South Qala Fault (SQF)

Along the western, micrite-dominated fault trace of the SQF, the most widespread change in texture between host and fault rock is related to fluid rock interactions. Increased cementation is commonly observed in the region between parallel slip surfaces. The calcite cements occlude both inter- and intra-granular porosity and appear to be formed of an early microcrystalline calcite followed by a later microspar calcite (Figure 9C). Cementation is relatively continuous along the length of the exposure.

Fault breccia is characterised by clasts of host rock within a fracture mesh, typically composed of intact globigerina grains, and fragments of cataclased bioclasts (predominantly skeletal fragments). Open fractures are common, often within a localised region of grain size reduction, indicating localised cataclasis along minor slip planes (Figure 9E). Breccia clasts are also commonly bound by open fractures, containing cements in certain regions (Figure 9A & D), along with minor calcite twinning (Figure 9B).

Beds that have higher proportions of coarser grained bioclasts, such as benthic foraminifera and bivalves, exhibit more cataclasis (grain fracturing and comminution) than those dominated by globigerina fossils. However, more pervasive cataclasis only occurs within several millimetres of the principal slip surface (Figure 9F).

The Xlendi member of the LCL along the eastern fault segment shows a more typical cataclasite veneer, bound by parallel slip surfaces, in which grain size is reduced relative to the host rock through grain comminution (Figure 10A). Calcite cements have occluded the majority of the pore spaces immediately adjacent to these slip surfaces, behind which pore spaces remain open. Regions of the slip surface exhibit brecciation, in which individual coarse grained bioclasts, or large bioclast fragments, behave as host clasts within a comminuted fracture mesh (Figure 10B). At the western tip of the slip surface is a *c.*10-30 cm thick band of deformed Xlendi member that is fine grained and composed of comminuted grains fitting the description of an uncemented cataclastic fault rock.

‘figure 9 here’

‘figure 10 here’

3.2.3. Qala Point Fault Zone (QPFZ)

Despite the grain-dominated fabric of the host rocks, there is limited cataclastic fault rock development within the QPFZ. A short section of the principal slip surface contains a thin hanging wall veneer of fine grained Xlendi fault rock, behind which are regions of increased cementation (Figure 11B). The fine-grained veneer contains clasts of low porosity cataclased bioclasts (Figure 11E) and a matrix consisting of intact bioclasts, or 'survivor bioclasts', surrounded by 2 generations of calcite cement (Figure 11E); an initial Fe-rich cryptocrystalline micrite cement surrounds the clasts and a sparry calcite cement fills the remaining voids. Dolomite cements are observed within intragranular pore spaces (Figure 11E). These dolomite cements are only observed within principal slip surface fault rocks. Additionally, the southern bounding slip surface contains a thin (*c.*1 cm) veneer of cataclasite (Figure 11A & D), in which cataclasis and cementation has resulted in a reduced porosity and a reduction in grain size (Figure 11D). Fossil bioclasts have become rounded during faulting and are surrounded by a matrix of fine grained clastic fragments or cements that appear dark in optical micrographs (Figure 11D). However, unlike the principal slip surface cataclasite veneer, there is no cemented matrix.

In contrast to the Xlendi member, the Attard member does not appear to exhibit grain scale cataclastic deformation. However, fault breccia is widespread along the principal slip surface and subsidiary slip surfaces. Breccia clasts are subrounded to subangular, range in size from mm scale up to 50 cm, and are poorly sorted with highly heterogeneous microstructures (Figure 12C). Two primary forms of fault breccia can be observed within the fault zone; fault breccia consist of either undeformed clasts of host rock, often with cemented pore spaces, or clasts that exhibit recrystallization. A fine grained fracture mesh, typical of cataclastic fault breccia, is not observed. Instead, diagenetic features and palaeosol features are commonly present between breccia clasts; breccia matrices are composed of Fe-rich cements, some of which have cemented pore spaces and show evidence of rhizogenic (root formed) microstructures (Figure 12C). Fractures are commonly filled with local scale brecciation, or contain regions of recrystallization (Figure 12D). A dark brown fault core, up to 7 cm thickness, is present between the Attard and Xlendi members along the principal slip surface. Optical micrographs show this core to be composed of pedogenic calcrete with rhizogenic microstructures.

‘figure 11 here’

‘figure 12 here’

4. Fault rock thickness and continuity

The ability to quantify fault rock distribution can be aided by 2 key metrics: fault rock thickness (FRT) and fault rock continuity (FRC). Fault rock thickness is highly variable over local scales (Figure 13). Thickness variability is particularly evident for fault breccia, due to the lensoidal geometries and fault zone architecture complexities (i.e. fault breccia is thicker at slip surface junctions). Therefore, fault breccia is characterised by poor FRC and thicknesses ranging from areas of absence to several meters. This is best observed along the 30 m and 90 m displacement faults (QPFZ and VLF, respectively). Cemented fault rocks and cataclasites have a reduced FRC, mean FRT, and thickness range relative to fault breccia.

Although these fault rocks still occur in lensoidal geometries, they are generally <0.5 m in thickness, thus reducing the range of thickness values. Cataclasite is relatively uniform in thickness with poor continuity at low displacements (Figure 14 & 15).

Although individual fault rock types have poor continuity, the total fault core continuity is relatively high for each of the 3 fault zones shown in Figure 13. FRC is approximately 1 along the principal slip surface, as shown by the FRC value for the combined principal slip surface measurements from all 3 fault zones (Figure 13). In these examples, although overall continuity of fault rock appears lowest on the highest (90m) displacement fault (VLF, Figure 13 bottom right), this is principally due to the distributions of fault breccia on both principal and subsidiary slip surfaces in the increasingly complex fault zones. Hence it does not indicate a more general trend with fault displacement.

Cataclasite continuity appears be significantly lower for the 90 m displacement fault relative to the 50 m displacement fault (Figure 13). However, cataclasite FRT and FRC measurements from all 6 fault zones show there to be a positive correlation with increasing displacement for both metrics (Figure 15). The displacement hosted by just the principal slip surface of the fault zones with highly complex, distributed damage zones (30 m and 90 m displacement) is less than the total fault zone displacement. Therefore, the cataclasite FRC values appear to lie to the right of the trend, such that the values are closer to the trend when considering only the displacement across the principal slip surface (highlighted by black arrows in Figure 15).

‘figure 13 here’

‘figure 14 here’

‘figure 15 here’

5. Discussion

5.1. Controls on deformation

Fault zone architecture is highly variable throughout the studied fault zones. At the QPFZ, the dextral component to slip combined with the complex nature of the fault zone architecture, comprising of multiple slip surfaces sub-parallel to the principal slip surface, multiple pull apart structures, and Riedel shear fractures, suggests that the fault zone is likely part of a dextral flower structure or fault stepover (e.g. McClay et al. 2001). This architecture promotes distributed deformation, with several slip surfaces accommodating a portion of the strain, and encourages discontinuous fault rock distribution. Dilatational fault jogs also lead to a discontinuous fault rock distribution (primarily fault breccia). This indicates that the tectonic setting of the QPFZ (30 m displacement) is likely to have some control over fault rock distribution, whereby the small scale en echelon wrench system within the larger scale structure of the SGF leads to a distributed damage fault zone, characterised by poor FRC (Figure 13). Further to this, the host rock porosity also influences the architecture; in the QPFZ, subsidiary slip surfaces are primarily located within the low porosity footwall of the fault zone, where deformation is more prone to extensional and shear fracturing relative to the higher porosity hanging wall.

In contrast to the distributed damage zone of the QPFZ, the SGF and LCL slip surface of the SQF have a more typical fault zone architectures (e.g. Chester and Logan 1986, Caine et al., 1996), hosting localised fault cores surrounded by a damage zone. The host porosity for both the Xlendi member (LCL) and the UCL is relatively high, making them more prone to granular flow and cataclasis on the grain scale, which promotes localised deformation along a single principal slip surface.

The architectures described are intrinsically linked to the observed deformation mechanisms. Widespread fault breccia formation is limited to the micrite-dominated footwall of the SQF and to the low porosity Attard member hanging wall of the QPFZ. Whilst breccias consistently occur in discrete, discontinuous lenses, there appears to be numerous mechanisms by which they form. At the SQF, lenses of fault breccia correlate with fault irregularities or corrugations. This suggests that fault breccia lenses may be the result of either dilation, due to void spaces created from fault geometries, creating hydraulic implosion breccia (Sibson 1986; Woodcock et al., 2007), or increased strain during fault linkage (Fossen et al., 2005; Joussineau and Aydin, 2007); during the initial stages of fault growth, overlapping or right stepping fault segments link to form lenses of increased dilation or strain in which fault breccia can form (Figure 7E). Further breccia formation appears to occur due to the entrainment of beds along the fault zone, whereby the entrained GL beds have been subject to mechanical abrasion from frictional sliding, thus resulting in intense fracturing and brecciation (Figure 5F) (Sibson, 1986). At the QPFZ, through going slip surfaces and sharp contacts between breccia and host rock suggest fault breccia is formed via either the coalescence of multiple slip surfaces or through the creation of void space relating to fault geometries. However, the rhizogenic structures present within the breccia matrix either overprints any initial fault related fracture mesh or suggests breccia has formed via karst collapse processes (e.g. Kerans 1993; Wright et al. 2009). Ultimately, the mechanical weathering potential of root wedging means the extent of fault related brecciation is difficult to determine at the QPFZ.

In contrast to fault breccia formation, cataclastic deformation is limited to specific lithologies. In general, cataclastic fault rock is poorly developed within both the high porosity micrite-dominated SQF slip surface and within the low porosity grain-dominated QPFZ footwall. Within the QPFZ, cataclasis is only observed in the higher porosity grain-dominated Xlendi member. However, there is no extensive cataclasite observed at outcrop. Conversely, cataclasis is common and well developed in high porosity grain-dominated wall rocks, such as the SGF and the Eastern fault trace of the SQF. This indicates that the high initial host rock porosity is a key factor in determining whether cataclasis will occur, as has been suggested in previous literature (Wong et al., 1997; Billi et al., 2003). However, the micrite-dominated GL does not exhibit cataclastic deformation, despite the high initial porosity (>30%), indicating that there are additional controls on which deformation mechanisms occur. The GL is weaker, finer grained, and more homogeneous than the grain-dominated lithologies. This leads to dispersed deformation within the GL, through fracturing and brecciation (Michie 2015). This indicates that the presence of large, high strength bioclasts within the Xlendi member (LCL) and the UCL also plays a part in allowing them to deform via granular flow and cataclasis.

The cataclasite fault rocks observed on Malta commonly have surviving bioclasts within a fine-grained matrix of fractured fossils and microcrystalline cements (Figure 7, 9 & 11). The surviving grains show less apparent grain fracturing or comminution than the surrounding fine grained matrix. Bioclasts that deform more readily appear to consist of planktonic foraminifera and skeletal fragments with large intragranular pore spaces. Conversely, bioclasts that are more resistant to deformation appear to consist of fossils such as echinoderms, which have stronger radial cell walls and little intragranular pore space. Preferential bioclast deformation is also commonly observed in the Attard Member, in which red algae (rhodolith) fossils appear to resist deformation, due to their fine scale cellular internal structure that prevents large intragranular pores, thus increasing the fossils resistance to pore collapse. This selective deformation implies that fossil content (i.e. carbonate age and facies) may have a control on deformation style within a fault zone, hence controlling fault permeability.

In addition to lithological controls, the extent to which cataclasis occurs, and its distribution, is partially controlled by the fault zone architecture. For example, the cataclasite veneer along the QPFZ hanging wall slip surface is poorly continuous due to the distributed damage zone (Figure 15). The proximity to the intersection between the SGF and the SQF indicates a region of increased strain at the fault junction, which may contribute to deformation band formation; single tip fault intersections have been shown to exhibit complex and extensive subseismic deformation (Fossen et al., 2005). The timing of faulting relative to deposition may also have influenced deformation band formation at the SGF. Faulting occurred early during deposition of the UCL (Dart et al., 1993), therefore sediments had undergone limited diagenesis, had a higher initial porosity, and were likely poorly lithified. Therefore, granular flow can easily occur, leading to a high intensity of deformation bands that exhibit a reduced porosity, reduced grain-size and grain translation (Figure 8). Minor pressure solution seams and sutured grain boundaries around individual fossil clasts suggest increased cementation within the deformation bands is partly a result of diffusive mass transfer in addition to the preferential disaggregation of the weakest bioclasts. Deformation bands increase in intensity towards the principal slip surface, where a fault core of several centimetres thick is produced by similar processes.

5.2. Controls on FRT and FRC

The continuity of fault rock is important when considering any across-fault fluid flow. For clay bearing siliciclastic rocks, shale gouge ratio and shale smear factor (Yielding et al., 1997) provide a first order approach to this. However, for carbonate rocks this is not applicable. Utilising field studies to draw relationships between fault rock continuity, fault rock thickness, host texture, and fault zone architecture can aid the better prediction of FRC, FRT and thickness variability in the subsurface. The data shown in this study indicates that displacements in the range of 50 – 200 m are required for continuous grain scale cataclasite fault rock to form within high porosity carbonate-hosted fault zones. Whilst other forms of fault core may also restrict fluid flow, carbonate-hosted cataclasites have been shown to exhibit low permeability values (e.g. Micarelli et al. 2006; Agosta et al. 2007; Bauer et al., 2016; Michie & Haines 2016). Hence, is important to be able to predict when a cataclastic fault core may become continuous.

Although a FRC value <1 may impact flow over production timescales, it is highly unlikely to impact fluid flow over geological time. However, the uncertainty regarding FRC estimates from the methods used in this study means determining whether a fault core is fully continuous from outcrop data alone is unrealistic. Hence, determining FRC from field measurements can only be used as a first order approach to considering fault rock distributions. The limitations of this method of quantifying FRC are as follows (highlighted by Figure 16):

- The total recorded fault rock length assumes that all fault rock is mappable (i.e. fault rock has not been subject to sufficient weathering to either remove fault rock or make it poorly visible).
- The scale of fault zone exposure may be too small to capture patterns of fault rock distribution (Figure 16C).
- Fault rock may appear to be laterally continuous when studying fault zones that are exposed in map view (or only accessible along strike), however, the vertical distribution may be discontinuous. Therefore, a 3D fault exposure is ideal for calculating FRC.
- When studying a fault zone exposed in 3 dimensions, measuring the total fault rock length from a 2D map view may misrepresent FRC. This can be avoided by calculating FRC as a ratio of the area of fault rock coverage relative to the area of exposed fault surface (Figure 16D). If the exposure is not suitable for this, a horizontal plane can be projected across the fault surface, along which the total fault rock length can be measured. However, it is clear that the height of the plane on the slip surface will vary the estimated FRC value.
- It is often difficult to determine the fault rocks present behind a fault surface. Hence, a core plug drilled perpendicular to the fault surface is useful in determining FRC and FRT.

‘figure 16 here’

The QPFZ (30 m displacement), VLF (90 m) and the IMF (210 m) have apparently continuous fault cores. However, the fault cores are composed of multiple fault rock types, which when considered on their own are often discontinuous (Figure 13 & Figure 14). Due to the different fabrics of each of these fault rocks, they will each have different impacts on fluid flow. According to permeability data from the VLF (Michie & Haines 2016), cataclastic fault rock has a far greater sealing potential than any other fault rocks present within Maltese fault zones. As such, the continuity of cataclasite would likely be a key factor in determining whether a fault will behave as a barrier to fluid flow.

FRC data shows that for the fault zones exhibiting a distributed damage zone, namely the QPFZ and the VLF (30 m and 90 m, respectively), fault breccia is more continuous than cataclastic fault rock. Cataclasite is poorly developed within these fault zones (FRC = *c.*0.1 – 0.5) relative to the 50 m displacement fault at RiB (FRC = *c.*0.8) and the 210 m displacement IMF (FRC = *c.*1). The poor FRC of cataclasite within a distributed damage zone relates to the multiple slip surfaces that accommodate displacement and reduce the amount of strain localised along the principal slip surface. Therefore, a distributed damage zone can act as a buffer to cataclasite formation. This is further highlighted by Figure 14, from which it is evident that increasing displacement leads to better developed (i.e. thicker, more continuous) cataclasite, whilst a distributed damage zone is characterized by poor cataclasite continuity (i.e. the 30 m and 90 m displacement faults). The 50 m displacement fault has a similar architecture to the SQF, with a single localised Xlendi member slip surface. However, the lithofacies juxtaposition is the same as for the VLF; a GL hanging wall juxtaposed against an Xlendi footwall. The lack of a distributed damage zone may be due to strain accommodation via the formation of an intense array of deformation bands in the hanging wall, as described by Rotevatn et al. (2016), combined with the junction with a series of conjugate slip surfaces that are parallel to the principal orientations of this deformation band array. Due to there being no distributed damage zone, cataclasite at the 50 m displacement fault zone is more continuous than for the 30 m and 90 m displacement fault zones (FRC = 0.8, 0.15, and 0.47 respectively).

FRT clearly exhibits significant variability over the scales recorded in this study. However, average thicknesses show a trend of increasing thickness with increasing displacement. Fault breccia is consistently the thickest fault rock fabric present within the fault zones. The nature of fault breccia distribution explains the large variability in thicknesses; fault breccia occurs in lenses, the thickness of which corresponds to whether breccia is formed via shearing of fault surface asperities, the filling of fault jogs, or fault linkage. Cataclasite FRT falls below the interquartile range of the total fault rock thickness for all 3 fault zones shown in Figure 13. Thicknesses appear to become less variable with increasing displacement where cataclasite is present (Figure 14). This may be explained by a more variable strain distribution along a slip surface during the initial stages of faulting, or greater localisation of strain over larger displacements.

5.3. Comparisons with other fault zones

To determine whether the relationships between host rock, deformation mechanisms and architectural characteristics of the studied fault zones are applicable to fault zones within different carbonate sequences, comparisons with previous field-based studies are highly valuable. A number of studied fault zones exhibit some similarities to faulting in Malta, despite larger fault displacements, more complicated tectonic histories, and greater burial (e.g. Tondi et al., 2006; Agosta et al., 2007; Fondriest et al., 2015; Bauer et al., 2016; Demurtas et al., 2016). These fault zones commonly have continuous cataclastic fault cores, as would typically be expected along kilometre scale displacement faults. However the deformation mechanisms by which cataclasis occurs, and therefore the resulting cataclasite textures, often differs to that of Malta. Cataclasites in these fault zones tend to result from pervasive fracturing, creating lithons that reduce in size down to the millimetre scale at the principal slip surface. Often there is little-no evidence of shearing, indicating that deformation is a result of in-situ coseismic shattering (Fondriest et al., 2015; Demurtas et al., 2016). Architectural observations of these fracture-derived cataclasites (e.g. Bauer et al., 2016), and their absence from Malta, suggests that greater burial depths or greater fault displacements are required to form an extensive, continuous unit.

More porous dolomite clasts within the Foiana Fault Zone (Fondriest et al., 2015) display grain scale deformation through pore collapse and compaction, similar to that of the high porosity, grain-dominated deformation that occurs in Malta. Grain scale deformation within high porosity carbonates is further documented in fault zones with burial depths from 2 km (Tondi et al., 2006) down to <50 m (Tondi et al., 2006). This indicates that high porosity carbonates will likely deform through grain-scale cataclasis, independent of burial depth. Faulted high porosity calcarenites in southern Sicily (Micarelli et al., 2006) show there to be continuous fault core after 5 m. This is in contrast with fault zones in Malta, in which a fault core is not continuous until greater displacements (*c*.30 m for continuous fault rock (Michie and Haines, 2016) and 50 – 200 m for a continuous cataclastic fault core). This difference can likely be attributed to the lack of mechanical juxtapositions along the Sicilian faults, such that strain localization can occur along the cataclastic fault core at low displacements and create a continuous band of fault rock. Contrastingly, the juxtaposition of different lithofacies with differing mechanical and textural properties in Malta tends to produce more distributed deformation, thus inhibiting FRC until greater displacements.

Cataclasis in carbonate rocks is commonly accompanied by grain boundary pressure solution, documented at a variety of burial depths (e.g. Cilona et al., 2012; Viti et al., 2014; Rotevatn et al., 2016). Additionally, the presence of phyllosilicate material within the faulted stratigraphy have been shown to produce alternative fault rock textures to those observed in Malta. For example, the Pietrasecca Fault, central Apennines, hosts a 14 m thick fault core consisting of discontinuous lenses of fault breccia and cataclasite, both of which host a clayey matrix, and a central phyllosilicate-rich layer. The phyllosilicate material is suggested to have been injected into the fault zone from the overlying clay formations during seismogenic activity (Smeraglia et al., 2016). Although the Maltese stratigraphy hosts clay rich units, this is not observed within the studied fault cores, as the injection of soft rocks along fault zones is only possible at depth, when the ratio of rock strength to effective strength is sufficiently low to allow fluid into voids (van der Zee et al., 2003; van der Zee and Urai, 2005).

5.4. Impacts on fluid flow

Although fault cores are relatively continuous, it is clear that sub-seismic structures, such as restraining or releasing stepovers, breached relay zones, flower structures etc. are important when considering across-fault fluid flow; these structures are likely to be characterised by a distributed damage zone. In cases where a low permeability cataclastic fault core is predicted (e.g. 100 m displacement fault juxtaposing two high porosity grain-dominated carbonates), such structures may in fact act as cross fault leakage points that prevent reservoir compartmentalisation, assuming other fault rock products have negligible permeability variations relative to the host rock. However, other fault rock fabrics may also be associated with low permeability that could make up fault core and impede flow. The most notable of these fault rocks are recrystallized fault rocks and cemented fault breccia, in which the host pore network is occluded, thus characterized by a low permeability (Michie and Haines, 2016).

Based upon the fault rock microstructures observed, it is apparent that there is a variety of complex factors determining the fault rock fabric within carbonate fault zones. For high porosity grain-dominated units, such as the Xlendi member (LCL) and the UCL members, grain scale deformation is key in fault rock formation. This suggests that the high intergranular porosity at the time of faulting allows granular flow within the rock and cataclasis of individual grains, as opposed to pervasive fracturing that leads to fracture-derived cataclasite rocks. This is most likely to be the case at displacements >50 m, at which point continuous cataclastic veneers may be present (Figure 15). In contrast, lower porosity grain-dominated limestones, such as the Attard member (LCL), are likely to deform in a brittle manner, leading to fracture-derived fault rocks such as fault breccia, and, potentially, fracture derived cataclasite. The variety in fault breccia microstructures indicates there to be a variety in their corresponding petrophysical properties. However, poor continuity of fault breccia formations means the most likely impact on fluid flow is where lenses of permeable fault breccia link two reservoir formations, allowing cross or up fault leakage.

5.5. Implications for transmissibility multipliers

The prediction of a geologically realistic FRT value is of great importance for estimating fault transmissibility multipliers. Figure 17 shows the impact of fault rock thickness on the estimated transmissibility multiplier for the 90 m displacement VLF. Host permeability data is taken from Michie et al. (2017) and fault permeability (k_f) values of 0.001 mD – 1 mD (at each order of magnitude in between) are used to show the sensitivity of FRT for different k_f values. Typically, the determination of FRT is based upon empirical scaling relationships between FRT and fault displacement. The empirical database of Solum & Huisman (2017) is used to determine the global mean for both fault core and fault zone thickness for a 90 m displacement fault. Based upon the FRT measurements along strike of the VLF (Figure 13), the arithmetic mean of all field measurements (1.15 m) gives a FRT that is 0.65 m thicker than the mean fault core thickness for a 10-100 m displacement fault. According the empirical database, the fault core thickness range based on +/- 1 standard deviation for a 10-100 m displacement fault is 0.06 – 2 m, with 56 % of all documented fault cores being 0.1 – 1 m thick. The entire fault zone thickness for the VLF is >50 m (Michie et al., 2014), which is over 5 times thicker than the fault zone thickness value from the empirical database (10 m), but still falls within range for a 10-100 m displacement fault based on +/- 1 standard deviation of 2-55 m. Therefore, the thickness of the VLF falls at the upper end of carbonate-hosted faults documented globally, due to the presence of a distributed damage zone. For this example, a 0.75 m variation in thickness value between the global mean fault core thickness and the field derived FRT results in a maximum of *c.*0.24 variation in transmissibility multiplier. However, from the shape of the curves it is apparent that for a low displacement fault zone in which a thin fault core (< 0.3 m) is predicted, a slight variation in FRT results in a significant variation in transmissibility multiplier (Figure 17). In accordance with the global database, this example highlights how a generalised displacement- fault rock thickness scaling relationship may not be appropriate for the estimation of transmissibility multipliers.

For fault a fault core with a very low permeability (< 10^{-3} mD), even a thin core of several centimetres may be sufficient to impact flow over production timescales (Figure 17). However, for a fault zone exhibiting a heterogeneous FRT, the regions with the thinnest FRT may act as leakage points over production timescales if permeability is not sufficiently low, even if the fault core is continuous. On a local scale, the mean transmissibility multiplier may be sufficiently low to suggest a barrier or partial barrier to fluid flow, but the thinnest regions may have transmissibility multipliers approaching 1, such that the fault has little or no impact on fluid flow, yet a compartmentalizing fault was predicted. This would prevent reservoir compartmentalisation over geological time. Similarly a heterogeneous fault zone with a FRC < 1 may act in a similar manner due to individual leakage points along the length of the fault. Along with the variability in documented FRT values (Solum and Huisman, 2017), this highlights the importance in considering FRC and FRT variations within fault zones. Utilising existing relationships between carbonate lithofacies juxtapositions, fault zone architecture, and the resultant fault rock style (Michie et al., 2014), the ability to predict a distributed damage zone may enable better predictions of fault zone heterogeneity and ultimately better predictions of fault permeability within faults hosting displacements on the order of meters to tens of meters.

'figure 17 here'

6. Conclusions

Three fault zones from the Qala Point region of Gozo, Malta, show a variety of fault rock fabrics and fault zone architectures, largely controlled by host lithofacies. Fault zones with high porosity wall rock (>15%), such as the SGF and the grain-dominated SQF segment, exhibit a single localised slip surface with well-developed cataclasite veneers, as well as often forming deformation bands within the damage zone surrounding the principal slip surface.

However, the presence of a distributed damage zone acts as a buffer to cataclastic deformation, such as the Xlendi member at the QPFZ, in which cataclastic fault rock is poorly developed. Cataclasite fault rocks and deformation bands form primarily by grain scale cataclasis, granular flow and grain translation. Pressure solution and cementation act to occlude remnant cataclasite porosity. Cataclasites found in Malta are typically grain scale cataclasites, in contrast to fracture derived cataclasites commonly observed in low porosity carbonates. This is attributed to the high porosity at the time of faulting, the coarse grained nature of some lithofacies, and shallow burial. Deformation appears to have been aided by poorly lithified sediments at the time of faulting, promoting deformation band formation. Grain scale cataclasis promotes preferential bioclast deformation, whereby weaker grains or fossils deform more readily than stronger grains. However, increased displacements may lead to the addition of other deformation mechanisms.

Fault zones with low porosity, grain-dominated wall rock (<15%), such as the Attard member at the QPFZ, or high porosity, micrite-dominated rocks, such as the GL member at the SQF, are less prone to cataclastic deformation at low displacements, favouring distributed deformation through extensional fracturing and the formation of fault breccia. Fault breccia formation mechanisms include hydraulic implosion breccia mechanisms related to lithofacies type, the filling of void spaces relating to fault geometries, the shearing of fault asperities, coalescence of slip surfaces and fault stepover linkage resulting in zones of increased internal strain.

Estimating fault rock continuity (FRC) in any fault zone is key to determining the sealing capacity of the fault. Although fault core is commonly continuous over outcrop scales, low permeability cataclastic fault rock in high porosity, shallow burial granular limestones only become continuous at 50-200 m displacement in this setting. The presence of a distributed damage zone appears to create a buffer in cataclastic rock formation, hence greater fault displacements are required to achieve a continuous cataclasite veneer. For example, the QPFZ shows a distributed damage zone due to the complex dextral wrench system creating numerous slip surfaces, whereby deformation is distributed across multiple sip surfaces. However, these observations are only valid for faults with <90 m displacement. Fault breccia is often more continuous than cataclastic fault rocks in low displacement faults or where there is a distributed damage zone. Further to FRC impacting across-fault fluid flow, FRT estimates can be used towards creating more realistic and site specific calculations of transmissibility multipliers to be used in reservoir models.

Acknowledgements

We thank Wintershall, ENI and ADMA for project funding and support. Partial project funding was also provided by NERC. The authors would also like to thank Andrea Billi and an anonymous reviewer for providing constructive reviews, which helped to improve the quality of this manuscript.

References

Agosta, F., 2008. Fluid flow properties of basin-bounding normal faults in platform carbonates, Fucino Basin, central Italy. Geological Society, London, Special Publications 299, 277–291.

Agosta, F., Kirschner, D.L., 2003. Fluid conduits in carbonate-hosted seismogenic normal faults of central Italy. Journal of Geophysical Research 108, 2221.

Agosta, F., Prasad, M., Aydin, A., 2007. Physical properties of carbonate fault rocks, fucino basin (Central Italy): implications for fault seal in platform carbonates. Geofluids 7, 19–32.

Antonellini, M., Aydin, A., 1994. Effect of faulting on fluid flow in porous sandstones: petrophysical properties. AAPG Bulletin 78, 355–377.

Aydin, A., Johnson, A., 1978. Development of faults as zones of deformation bands and as slip surfaces in sandstones. Pure and Applied Geophysics 116, 931–942.

Bauer, H., Schröckenfuchs, T.C., Decker, K., 2016. Hydrogeological properties of fault zones in a karstified carbonate aquifer (Northern Calcareous Alps, Austria). Hydrogeology Journal 24, 1147–1170. https://doi.org/10.1007/s10040-016-1388-9

Billi, A., Salvini, F., Storti, F., 2003. The damage zone-fault core transition in carbonate rocks: implications for fault growth, structure and permeability. Journal of Structural Geology 25, 1779–1794.

Birkle, P., Angulo, M., 2005. Conceptual hydrochemical model of late Pleistocene aquifers at the Samario – Sitio Grande petroleum reservoir, Gulf of Mexico, Mexico. Applied Geochemistry 20, 1077–1098. https://doi.org/10.1016/j.apgeochem.2005.01.013

Boccaletti, M., Cello, G., Tortorici, L., 1987. Transtensional tectonics in the Sicily Channel. Journal of Structural Geology 7, 869–876.

Bockel-Rebelle, M.-O., Hassall, J.K., Silva, F.P., Lozano, J.A., Al Deeb, M., El Abd Salem, S., Vesseron, M., Al Mehsin, K., 2004. Faults, fracture corridors and diffuse fracturing: ranking the main structural heterogeneities within onshore Abu Dhabi fields. 11th Abu Dhabi International Petroleum Exhibition and Conference. SPE 88676.

Bonson, C.G., Childs, C., Walsh, J.J., M.P.J., S., & Carboni, V., 2007. Geometric and kinematic controls on the internal structure of a large normal fault in massive limestones: The Maghlaq Fault, Malta. Journal of Structural Geology 29, 336–354.

Bosence, D.W.J., Pedley, H.M., 1982. Sedimentology and palaeoecology of a Miocene coralline algal biostrome from the Maltese Islands. Palaeogeography, Palaeoclimatology, Palaeoecology 38, 9–43.

Brandano, M., Frezza, V., Tomassetti, L., Pedley, M., Matteucci, R., 2009. Facies analysis and palaeoenvironmental interpretation of the Late Oligocene Attard Member (Lower Coralline Limestone Formation), Malta. Sedimentology 56, 1138–1158.

Caine, J.S., Evans, J.P., Forster, C.B., 1996. Fault zone architecture and permeability structure. Geology 24, 1025–1028.

Chester, F., Evans, J., Biegel, R., 1993. Internal structure and weakening mechanisms of the San Andreas Fault. Journal of Geophysical Research 98, 771–786.

Chester, F.M., Logan, J.M., 1986. Implications for mechanical properties of brittle faults from observations of the Punchbowl Fault Zone, California. Pure and Applied Geophysics 124, 79–106.

Childs, C., Manzocchi, T., Walsh, J.J., Bonson, C.G., Nicol, A., Schöpfer, M.P.J., 2009. A geometric model of fault zone and fault rock thickness variations. Journal of Structural Geology 31, 117–127.

Cilona, A., Baud, P., Tondi, E., Agosta, F., Vinciguerra, S., Rustichelli, A., Spiers, C.J., 2012. Deformation bands in porous carbonate grainstones: Field and laboratory observations. Journal of Structural Geology 45, 137–157. https://doi.org/10.1016/j.jsg.2012.04.012

Corona, F. V, Brauckmann, F., Beckmann, H., Gobi, A., Grassmann, S., Neble, J., Roettgen, K., 2012. Cross-fault pressure depletion, Zechstein carbonate reservoir, Weser-Ems area, Northern German Gas Basin. 3rd EAGE International Conference on Fault and Top Seals. Abstract A06.

Crawford, B.R., Myers, R.., Woronow, A., Faulkner, D.R., Rutter, E.H., 2002. Porosity-permeability relationships in clay-bearing fault gouge: Presented at the Society of Petroleum Engineers/International Society of Rock Mechanics, Rock Mechanics Conference, Irving, Texas, October 20-23,. SPE/ISRM 78214 13p.

Dart, C.J., Bosence, D.W.J., McClay, K.R., 1993. Stratigraphy and structure of the Maltese graben system. Journal of the Geological Society, London 150, 1153–1166.

Demurtas, M., Fondriest, M., Balsamo, F., Clemenzi, L., Storti, F., Bistacchi, A., Di, G., 2016. Structure of a normal seismogenic fault zone in carbonates: The Vado di Corno Fault, Campo Imperatore, Central Apennines (Italy). Journal of Structural Geology 90, 185–206. https://doi.org/10.1016/j.jsg.2016.08.004

Evans, J.P., Forster, C.B., Goddard, J. V., 1997. Permeability of fault-related rocks, and implications for hydraulic structure of fault zones. Journal of Structural Geology 19, 1393–1404.

Færseth, R.B., 2006. Shale smear along large faults: continuity of smear and the fault seal capacity. Journal of the Geological Society, London 163, 741–751.

Færseth, R.B., Johnsen, E., Sperrevik, S., 2007. Methodology for risking fault seal capacity: Implications of fault zone architecture. AAPG Bulletin 91, 1231–1246.

Fisher, Q., Knipe, R., 2001. The permeability of faults within siliciclastic petroleum reservoirs of the North Sea and Norwegian Continental Shelf. Marine and Petroleum Geology 18, 1063–1081.

Flodin, E., Gerdes, M., Aydin, A., Wiggins, W., 2005. Petrophysical properties and sealing capacity of fault rock, Aztec Sandstone, Nevada. In: R. Sorkhabi and Y. Tsuji, (Eds). Faults, Fluid Flow, and Petroleum Traps: AAPG Memoir 85, 197–218.

Fondriest, M., Aretusini, S., Toro, G. Di, Smith, S.A.F., 2015. Fracturing and rock pulverization along an exhumed seismogenic fault zone in dolostones: The Foiana Fault Zone (Southern Alps, Italy). Tectonophysics 654, 56–74. https://doi.org/10.1016/j.tecto.2015.04.015

Fossen, H., Johansen, T.E.S., Hesthammer, J., Rotevatn, A., 2005. Fault interaction in porous sandstone and implications for reservoir management; examples from southern Utah. AAPG Bulletin 89, 1593–1606. https://doi.org/10.1306/07290505041

Fossen, H., Schultz, R.A., Shipton, Z.K., Mair, K., 2007. Deformation bands in sandstone: a review. Journal of the Geological Society 164, 755–769.

Fulljames, J., Zijerveld, L., Franssen, R., 1997. Fault seal processes: systematic analysis of fault seals over geological and production time scales. In: Møller-Pedersen, P. Koestler, A. G., (Eds) Hydrocarbon Seals: Importance for Exploration and Production. Special Publication of the Norwegian Petroleum Society 7, 51–59.

Hull, J., 1988. Thickness-displacement relationships for deformation zones. Journal of Structural Geology 10, 431–435.

Illies, J.H., 1981. Graben formation - the Maltese Islands - a case history. Tectonophysics 73, 151–168.

John, C.M., Mutti, M., Adatte, T., 2003. Mixed carbonate-siliciclastic record on the North African margin (Malta) - coupling of weathering processes and mid Miocene climate. Geological Society of America Bulletin 115, 217–229.

Jolley, S.J., Dijk, H., Lamens, J.H., Fisher, Q.J., Manzocchi, T., Eikmans, H., Huang, Y., 2007. Faulting and fault sealing in production simulation models: Brent Province, northern North Sea. Petroleum Geoscience 13, 321–340.

Jongsma, D., Woodside, J.M., King, G.C.P., van Hinte, J.E., 1987. The Medina Wrench : a key to the kinematics of the central and eastern Mediterranean over the past 5 Ma. Earth and Planetary Science Letters 82, 87–106.

Joussineau, G. De, Aydin, A., 2007. The evolution of the damage zone with fault growth in sandstone and its multiscale characteristics. Journal of Geophysical Research 112, B12401. https://doi.org/10.1029/2006JB004711

Kerans, C., 1993. Description and interpretation of karst - related breccia fabrics, Ellenburger Group, West Texas. 181–200.

Kim, Y., Peacock, D.C.P., Sanderson, D.J., 2004. Fault damage zones. Journal of Structural Geology 26, 503–517.

Knai, T.A., Knipe, R.J., 1998. The impact of faults on fluid flow in the Heidrun Field. In: Jones, G., Fisher, Q. J. & Knipe, R. J. (eds) Faulting, Fault Sealing and Fluid Flow in Hydrocarbon Reservoirs. Geological Society, London, Special Publications 147, 269–282.

Knipe, R.J., 1992. Faulting processes and fault seal. In: Structural and Tectonic Modelling and Its Application to Petroleum Geology, R. M Larsen, H. Brekke, B. T. Larsen, E. Talleras (Eds.) Amsterdam, Elsevier 1, 325–342.

Lee, Y.-J., Wiltschko, D. V, Grossman, E.L., Morse, J.W., Lamb, W.M., 1997. Sequential vein growth with fault displacement: An example from the Austin Chalk Formation, Texas. Journal of Geophysical Research 102, 22611–22628.

Manzocchi, T., Walsh, J.J., Nell, P., Yielding, G., 1999. Fault transmissibility multipliers for flow simulation models. Petroleum Geoscience 5, 53–63. https://doi.org/10.1144/petgeo.5.1.53

Matonti, C., Lamarche, J., Guglielmi, Y., Marié, L., 2012. Structural and petrophysical characterization of mixed conduit/seal fault zones in carbonates: Example from the Castellas fault (SE France). Journal of Structural Geology 39, 103–121.

Mauldon, M., Dershowitz, W., 2000. A multi-dimensional system of fracture abundance measures. Geological Society of America Abstracts with Programs 32.

Mauldon, M., Dunne, W.M., Rohrbaugh, M.B., 2001. Circular scanlines and circular windows: new tools for characterizing the geometry of fracture traces. Journal of Structural Geology 23, 247–258.

Mcclay, K., Bonora, M., Mcclay, K., 2001. fault systems. AAPG Bulletin 85, 233–260.

Micarelli, L., Benedicto, A., Wibberley, C.A.J., 2006. Structural evolution and permeability of normal fault zones in highly porous carbonate rocks. Journal of Structural Geology 28, 1214–1227.

Michie, E.A.H., Haines, T.J., 2016. Variability and heterogeneity of the petrophysical properties of extensional carbonate fault rocks, Malta. Petroleum Geoscience 23. https://doi.org/10.1144/petgeo2015-027

Michie, E.A.H., Haines, T.J., Healy, D., Neilson, J.E., Timms, N.E., Wibberley, C.A.J., 2014.

Influence of carbonate facies on fault zone architecture. Journal of Structural Geology 65, 82–99.

Michie, E.A.H., Yielding, G., Fisher, Q.J., 2017. Predicting transmissibilities of carbonate-hosted fault zones. Geological Society, London, Special Publications 459.

Mitchell, T.M., Faulkner, D.R., 2009. The nature and origin of off-fault damage surrounding strike-slip fault zones with a wide range of displacements: A field study from the Atacama fault system, northern Chile. Journal of Structural Geology 31, 802–816.

Pedley, H.M., 1978. A new lithostratigraphical and palaeoenvironmental interpretation for the coralline limestone formations (Miocene) of the Maltese Islands. Overseas Geology and Mineral Resources 54, 1–17.

Pedley, H.M., Bennett, S.M., 1985. Phosphorites, hardgrounds and syndepositional solution subsidence: a palaeoenvironmental model from the Miocene of the Maltese Islands. Sedimentary Geology 45, 1–34.

Pedley, H.M., House, M.R., Waugh, B., 1976. The geology of Malta and Gozo. Proceedings of the Geologists' Association 87, 325–341.

Rawling, G.C., Goodwin, L.B., Wilson, J.L., 2001. Internal architecture, permeability structure, and hydrologic significance of contrasting fault-zone types. Geology 29, 43–46.

Reuther, C.-D., Eisbacher, G.H., 1985. Pantelleria Rift - crustal extension in a convergent intraplate setting. Geologische Rundschau 74, 585–597.

Riley, P.R., Goodwin, L.B., Lewis, C.J., 2010. Controls on fault damage zone width, structure, and symmetry in the Bandelier Tuff, New Mexico. Journal of Structural Geology 32, 766–780.

Rohrbaugh, M.B., Dunne, W.M., Mauldon, M., 2002. Estimating fracture trace intensity, density, and mean length using circular scan lines and windows. AAPG Bulletin 86, 2089–2104.

Rotevatn, A., Thorsheim, E., Bastesen, E., Fossmark, H.S.S., Torabi, A., Sælen, G., 2016. Sequential growth of deformation bands in carbonate grainstones in the hangingwall of an active growth fault: Implications for deformation mechanisms in different tectonic regimes. Journal of Structural Geology 90, 27–47. https://doi.org/10.1016/j.jsg.2016.07.003

Schlumberger, 2007. Schlumberger Market Analysis.

Shipton, Z., Cowie, P., 2001. Damage zone and slip-surface evolution over um to km scales in high-porosity Navajo sandstone, Utah. Journal of Structural Geology 23, 1825–1844.

Sibson, R.H., 1986. Brecciation processes in fault zones: inferences from earthquake rupturing. Pure and Applied Geophysics 124, 159–175.

Smeraglia, L., Aldega, L., Billi, A., Carminati, E., Doglioni, C., 2016. Phyllosilicate injection along extensional carbonate-hosted faults and implications for co-seismic slip propagation: Case studies from the central Apennines, Italy. Journal of Structural Geology 93, 29–50. https://doi.org/10.1016/j.jsg.2016.10.003

Smith, D.A., 1980. Sealing and Nonsealing Faults In Louisiana Gulf Coast Salt Basin. AAPG Bulletin 64, 145–172.

Solum, J.G., Huisman, B.A.H., 2017. Toward the creation of models to predict static and dynamic fault-seal potential in carbonates. Petroleum Geoscience 23. https://doi.org/10.1144/petgeo2016-044

Storti, F., Billi, A., Salvini, F., 2003. Particle size distributions in natural carbonate fault rocks: insights for non-self-similar cataclasis. Earth and Planetary Science Letters 206, 173–186.

Taylor, D.J., Dietvorst, J.P.A., 1991. The Cormorant Field, Blocks 211/21a, 211/26a, UK North Sea. Abbotts, I. L. (Ed.), 1991, United Kingdom Oil and Gas Fields, 25 Years Commemorative Volume, Geological Society Memoir No. 14. 73–81.

Tondi, E., Antonellini, M., Aydin, A., Marchegiani, L., Cello, G., 2006. The role of deformation bands, stylolites and sheared stylolites in fault development in carbonate grainstones of Majella Mountain, Italy. Journal of Structural Geology 28, 376–391.

van der Zee, W., Urai, J.L., 2005. Processes of normal fault evolution in a siliciclastic sequence: a case study from Miri, Sarawak, Malaysia. Journal of Structural Geology 27, 2281–2300. https://doi.org/10.1016/j.jsg.2005.07.006

van der Zee, W., Urai, J.L., Richard, P.D., 2003. Lateral clay injection into normal faults. GeoArabia 8, 501–522.

Vega Riveros, G., Saputelli, L., Patino, J., Chacon, A., Solis, R., 2011. Reserves estimation uncertainty in a mature naturally-fractured carbonate field located in Latin America. Offshore Technology Conference Brasil. OTC 22517.

Viti, C., Collettini, C., Tesei, T., 2014. Pressure solution seams in carbonatic fault rocks: mineralogy, micro/nanostructures and deformation mechanism. Contributions to Mineralogy and Petrology 167–970. https://doi.org/10.1007/s00410-014-0970-1

Wibberley, C.A.J., Shimamoto, T., 2003. Internal structure and permeability of major strike-slip fault zones: the Median Tectonic Line in Mie Prefecture, Southwest Japan. Journal of Structural Geology 25, 59–78.

Wibberley, C.A.J., Yielding, G., Di Toro, G., 2008. Recent advances in the understanding of fault zone internal structure: a review. In: Wibberley, C. A. J., Kurz, W., Imber, J., Holdsworth, R. E. & Collettini, C. (Eds). The Internal Structure of Fault Zones: Implications for Mechanical and Fluid-Flow Properties. Geological Society, London, Special Publications 299, 5–33.

Wiprut, D., Zoback, M.D., 2000. Fault reactivation and fluid flow along a previously dormant normal fault in the northern North Sea. Geology 28, 595–598.

Wong, T., David, C., Zhu, W., 1997. The transition from brittle faulting to cataclastic flow in porous sandstones: Mechanical deformation. Journal of Geophysical Research 102, 3009–3025.

Woodcock, N.H., Omma, J.E., Dickson, J.A.D., 2006. Chaotic breccia along the Dent Fault, NW England: implosion or collapse of a fault void? Journal of the Geological Society, London 163, 431–446.

Wright, V., Woodcock, N.H., Dickson, J.A.D., 2009. Fissure fills along faults: Variscan examples from Gower, South Wales. Geological Magazine 146, 890–902. https://doi.org/10.1017/S001675680999001X

Yielding, G., Freeman, B., Needham, D., 1997. Quantitative fault seal prediction. AAPG Bulletin 6, 897–917.

Figures

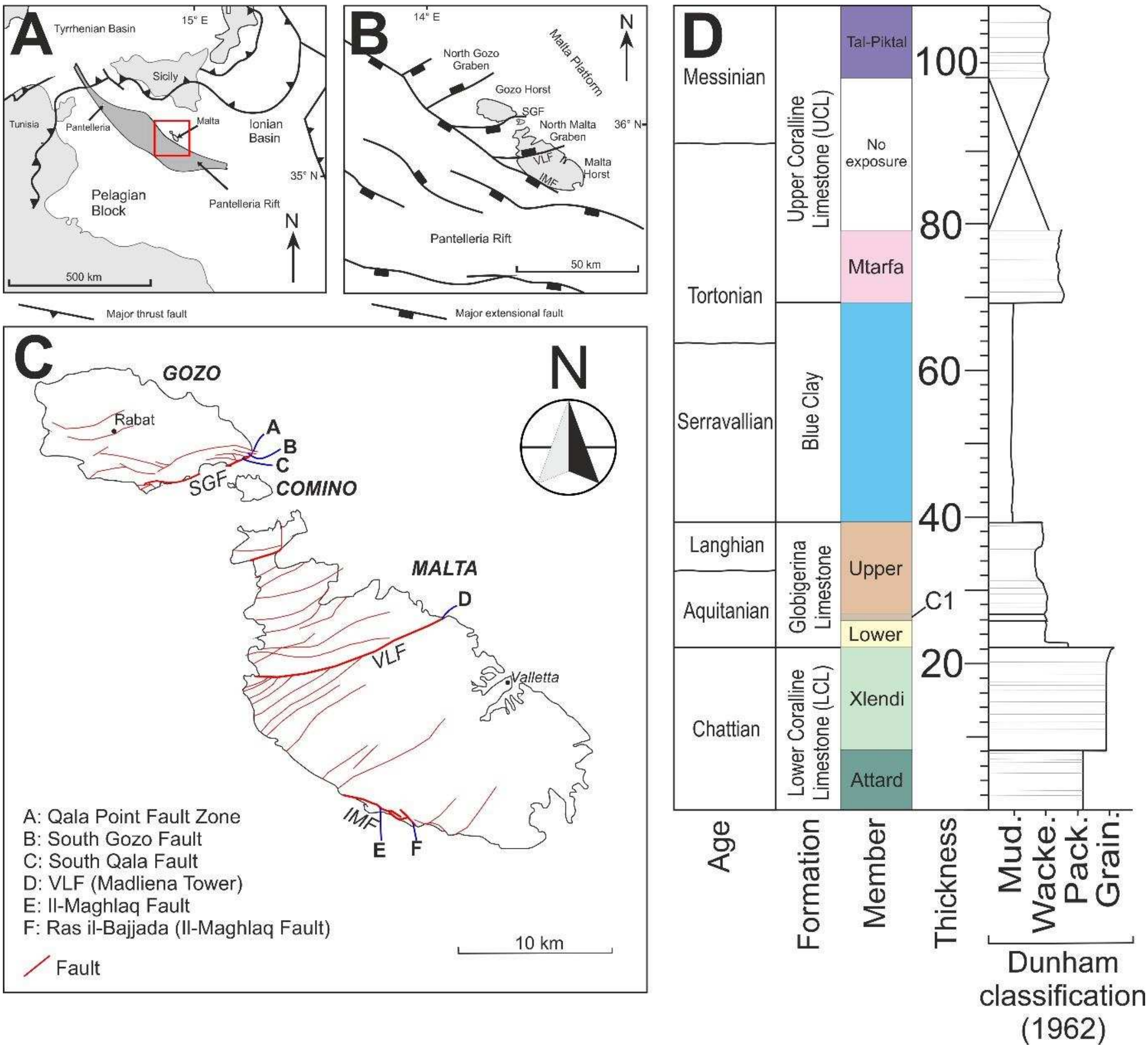

Figure 1: A) The location of the Maltese islands, on the northern shoulder of the Pantelleria Rift system, in the foreland of the Apennine-Maghrebian thrust system. B) Main structures of the Maltese island, oriented ENE-WSW and WNW-ESE, where the majority trends ENE-WNW (after Dart et al., 1993). SGF = South Gozo Fault; VLF = Victoria Lines Fault; IMF = Il–Maqhlaq Fault. C) Overview map of the Maltese Islands showing the locations of study sites (A-F). D) Stratigraphic log for the Qala point study area, eastern Gozo.

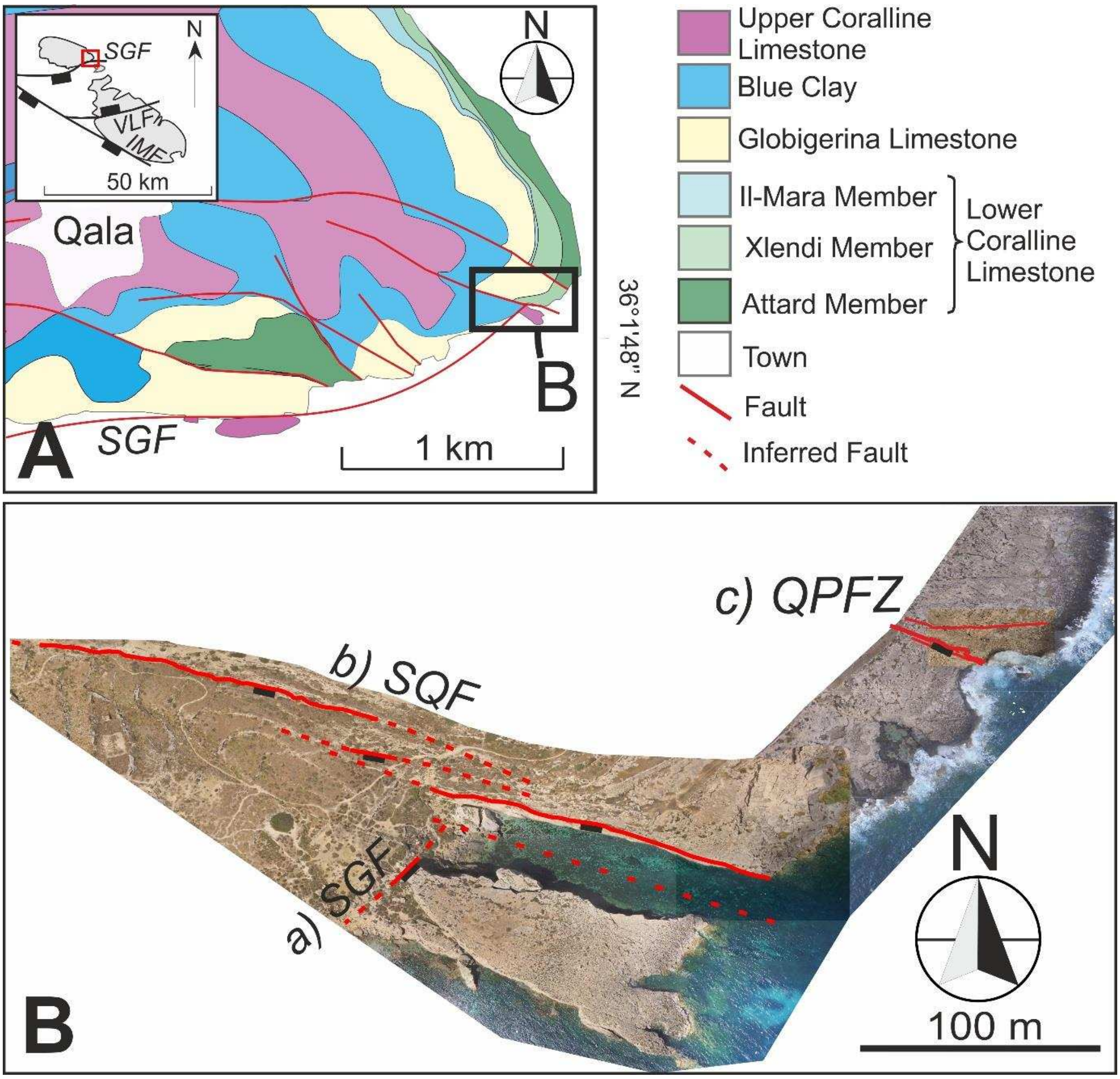

Figure 2: A) Geological map of the Eastern tip of Gozo (inset: map of Malta showing map location. Black box: location of the Qala Point study area). B) Drone map of the Qala Point study area with principal slip surfaces annotated. SGF = South Gozo Fault; SQF = South Qala Fault; QPFZ = Qala Point Fault Zone.

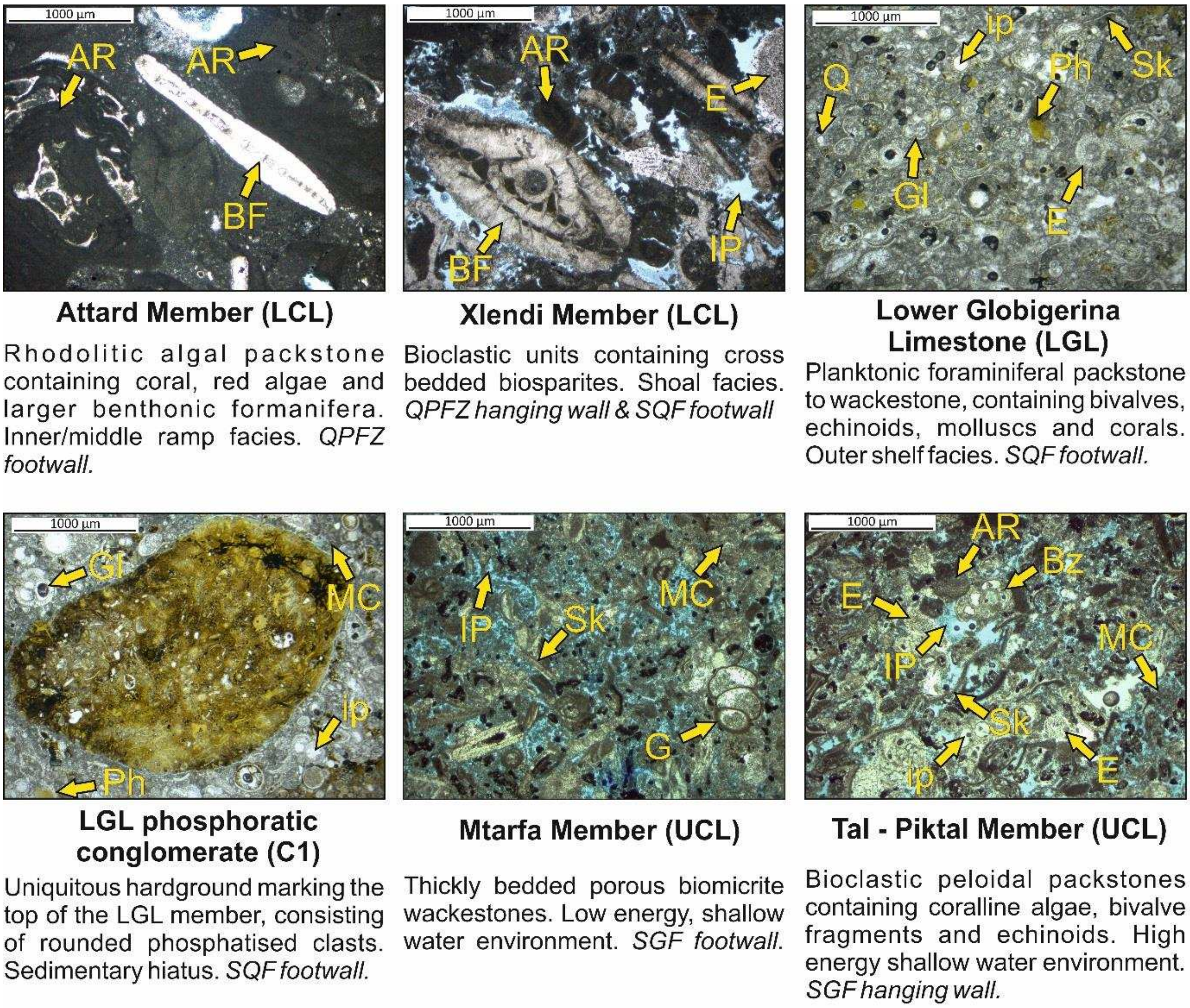

Figure 3: Host textures for the members of the Lower Coralline Limestone (LCL), the Lower Globigerina Limestone (LGL), and the Upper Coralline Limestone (UCL) present at outcrop. Optical micrographs in PPL with blue dyed epoxy resin used to highlight pore spaces. AR = Algal rhodolith; BF = Benthic foraminifera; Bz = Bryozoan; E = Echinoid; G = Gastropod; Gl = Globigerina; IP = Intergranular porosity; ip = Intragranular porosity; MC = Micrite cement; Ph = Ca-Phosphate; Q = Quartz; Sk = Skeletal fragments.

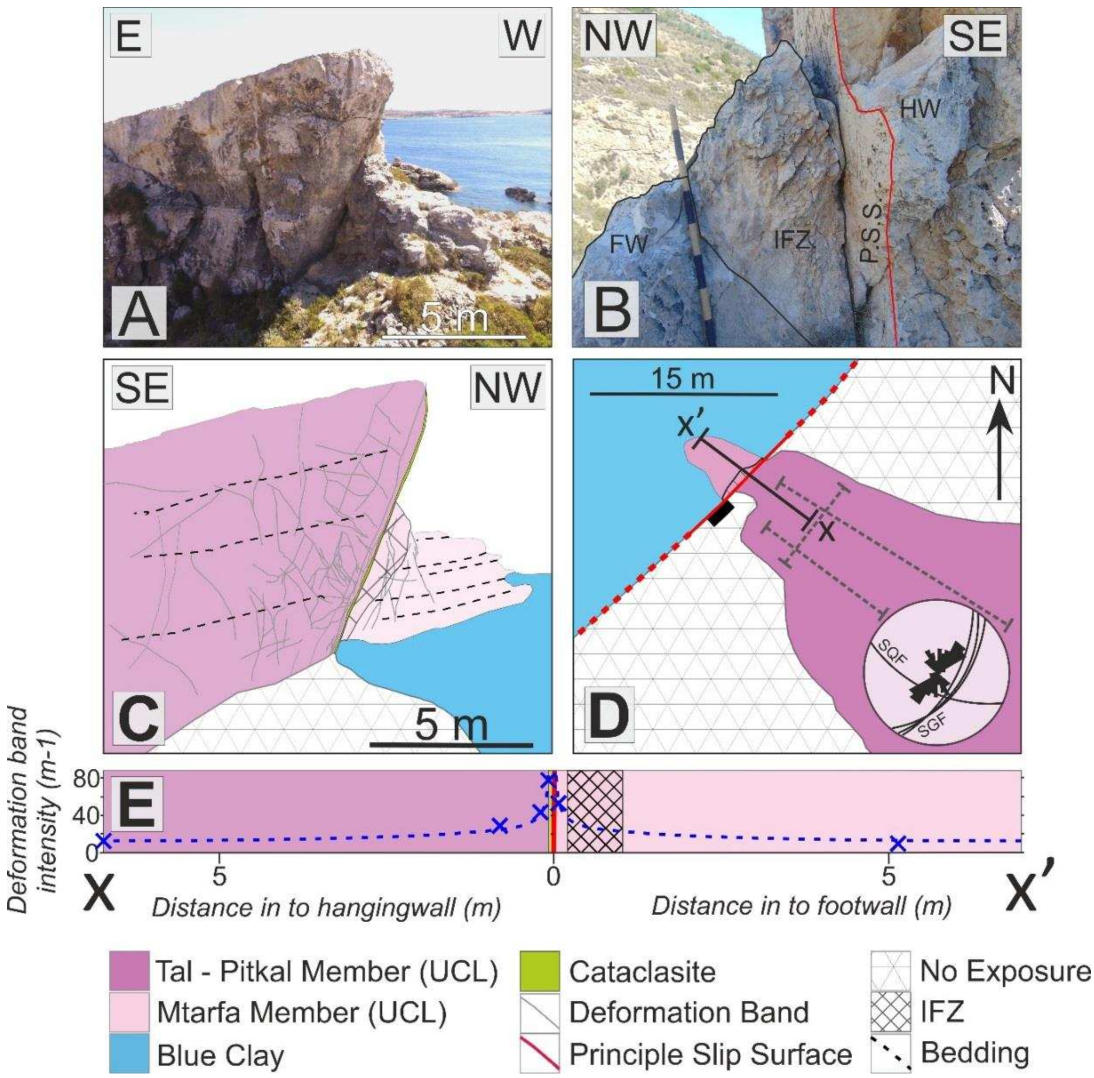

Figure 4: A) Cross sectional photo of the SGF outcrop at Qala Point. B) Close up photo (reverse view from A) of the SGF showing the intensely fractured zone (IFZ) of the footwall (FW) adjacent to the principal slip surface (PSS) and hanging wall (HW) hosting a cataclasite veneer. C) Geological cross section of the SGF at Qala Point (similar view to A). D) Map view of the SGF at Qala Point showing a lower hemispherical projection of the SGF and SQF faults together with deformation band orientations. Grey dashed lines represent scan line transects. E) Cross section (see D for location) showing deformation band intensity across the principal slip surface derived from field measurements and from individual samples (samples represented by crosses).

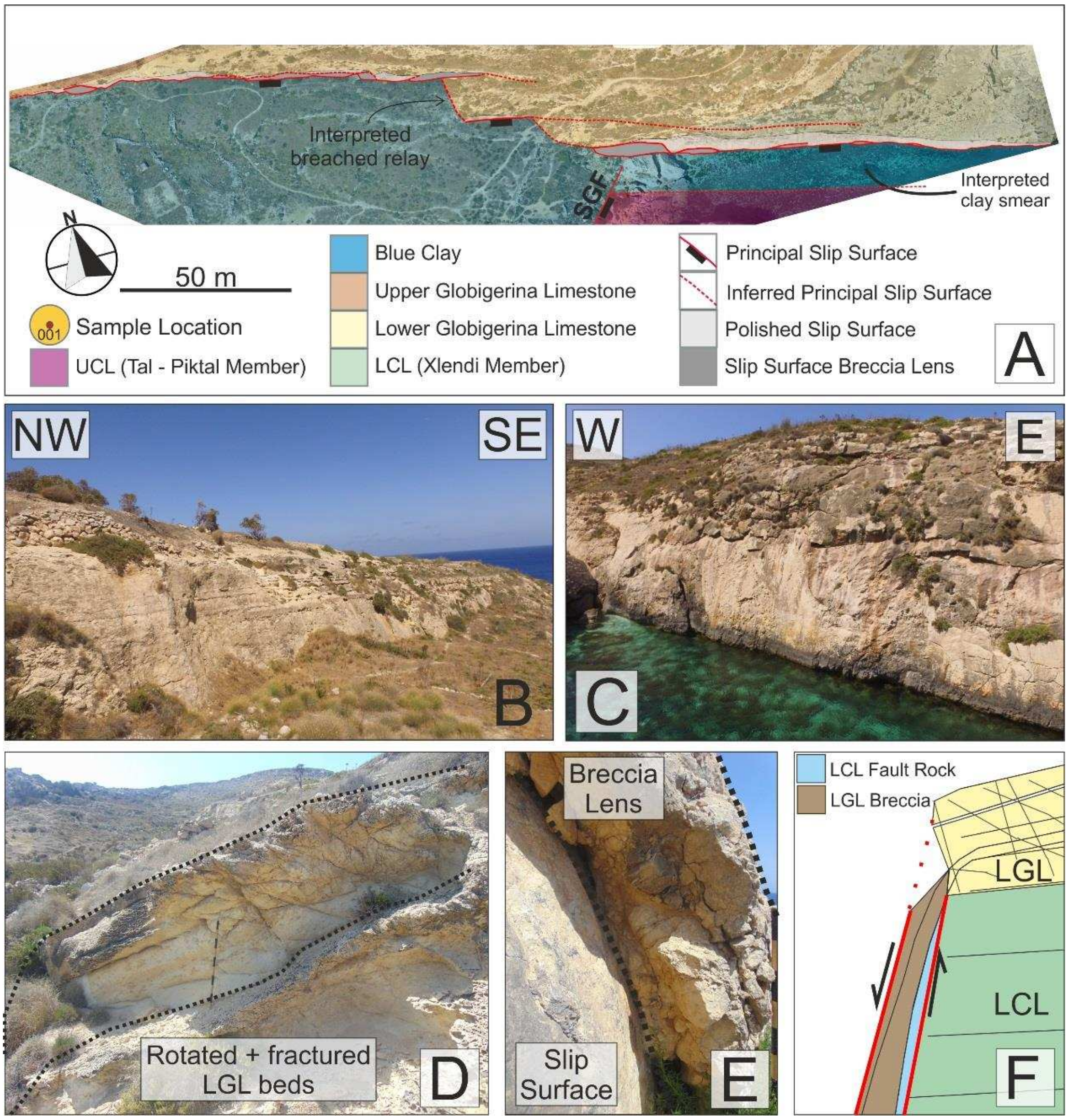

Figure 5: A) Geological map of the South Qala Fault (SQF) overlain on aerial drone map. B & C) photographs of the western Globigerina Limestone (GL) slip surface and eastern Lower Coralline Limestone (LCL) fault segments, respectively. D) Rotated and fractured GL bedding in the breached relay zone. E) Lens of brecciated GL bound by parallel slip surfaces, typical of the western fault segment. Here, the fault steps right and the 2 slip surfaces coalesce at the breccia lens tip. F) Schematic model of breccia formation; GL beds become increasingly fractured towards the fault, where they become rotated and entrained between parallel slip surfaces.

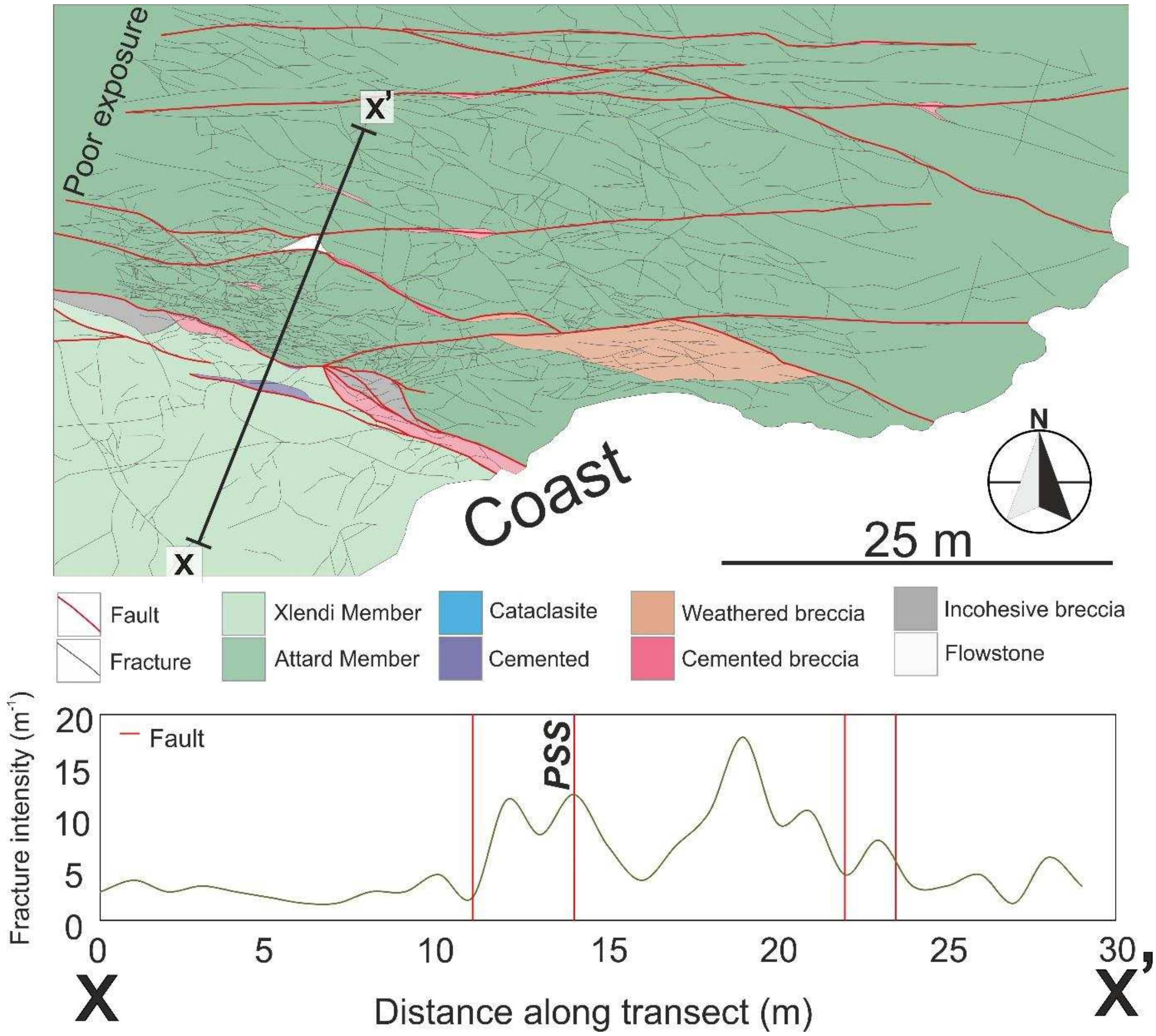

Figure 6: Top) Geological map of the Qala Point Fault Zone (QPFZ), showing fault rock distributions. Bottom) Linear transect across the QPFZ showing fracture intensity and the locations of slip surfaces (vertical red lines).

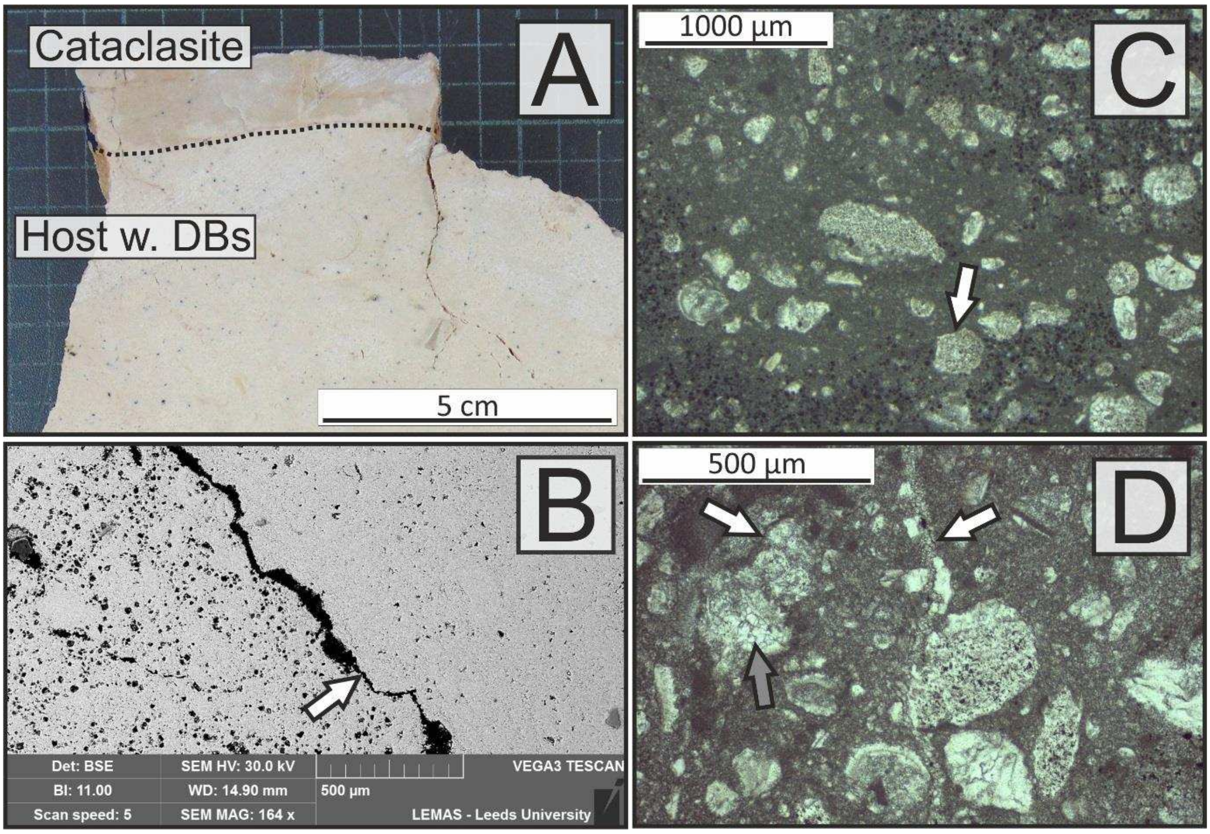

Figure 7: A) Hand specimen containing contact between cemented cataclasite and host rock containing deformation bands. B) BSE-SEM image of cemented cataclasite showing boundary between medium porosity and low porosity fault rock. Arrow indicates open pressure solution seam. C) Optical micrograph of a clast within cataclasite exhibiting reduced microporosity due to grain comminution. Bioclast boundary (arrow) shows a sutured grain boundary of an echinoderm at the contact with the clast, evidence of minor grain boundary pressure solution. Preferential bioclast deformation (e.g. mollusc and planktonic foraminifera fossils) has increased cryptocrystalline cement and reduced porosity (fossils such as echinoderms appear to be more resistant to deformation and have remained mostly intact). D) Optical micrograph of cemented cataclasite showing pressure solution seams (white arrows) and recrystallized bioclasts with sparry cements (grey arrow).

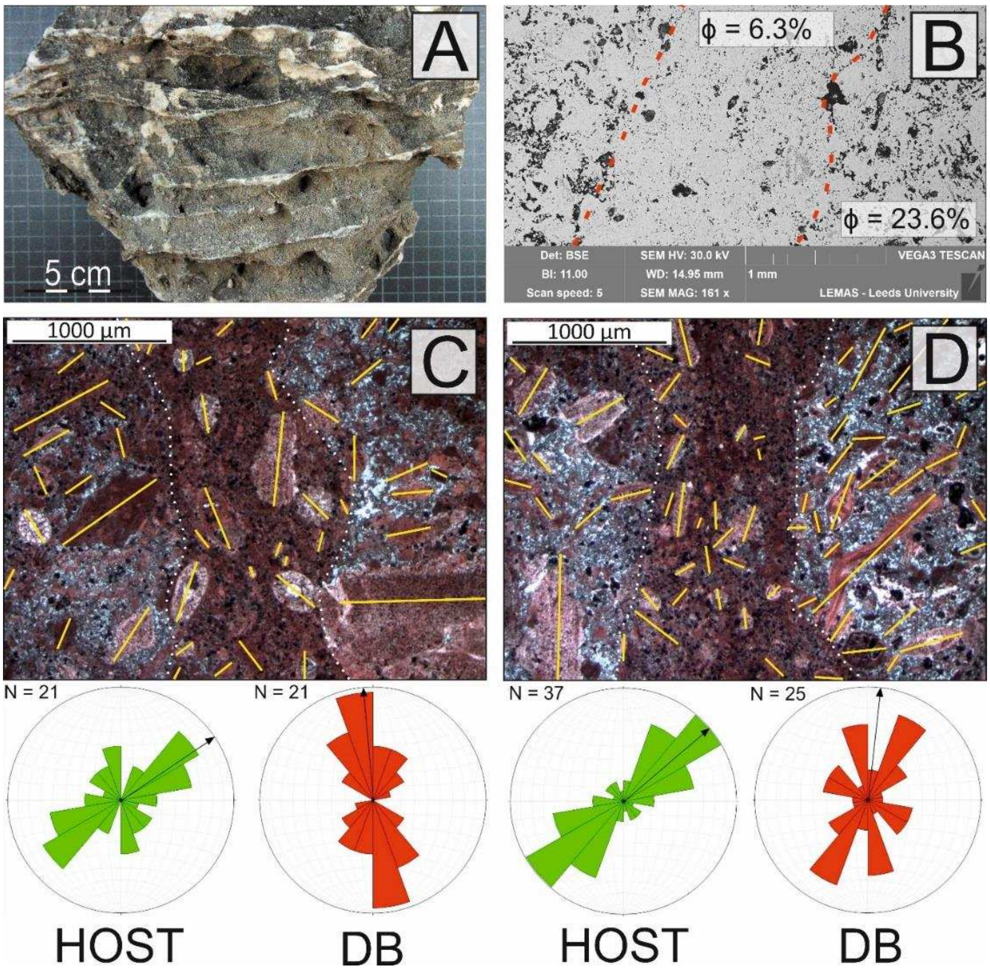

Figure 8: A) Hand specimen containing anastomosing deformation bands from the immediate SGF footwall. Deformation bands are less prone to weathering, hence form weathered ridges. B) BSE-SEM image of a deformation band from the sample shown in A. Red dashed line indicates the deformation band boundaries. Porosity estimated from image analysis is shown for the deformation band and surrounding sediment. C & D) Polished optical micrographs of deformation bands in the UCL, stained with Alizarin red S and potassium ferricyanide. Principal grain axes are shown by yellow lines, and their orientations are shown below for both the host and deformation band grains. The black arrows on the grain orientation plots indicate the mean orientation. Grains have been rotated and aligned parallel to the deformation band orientation. Increased micrite and microspar cements have reduced deformation band porosity.

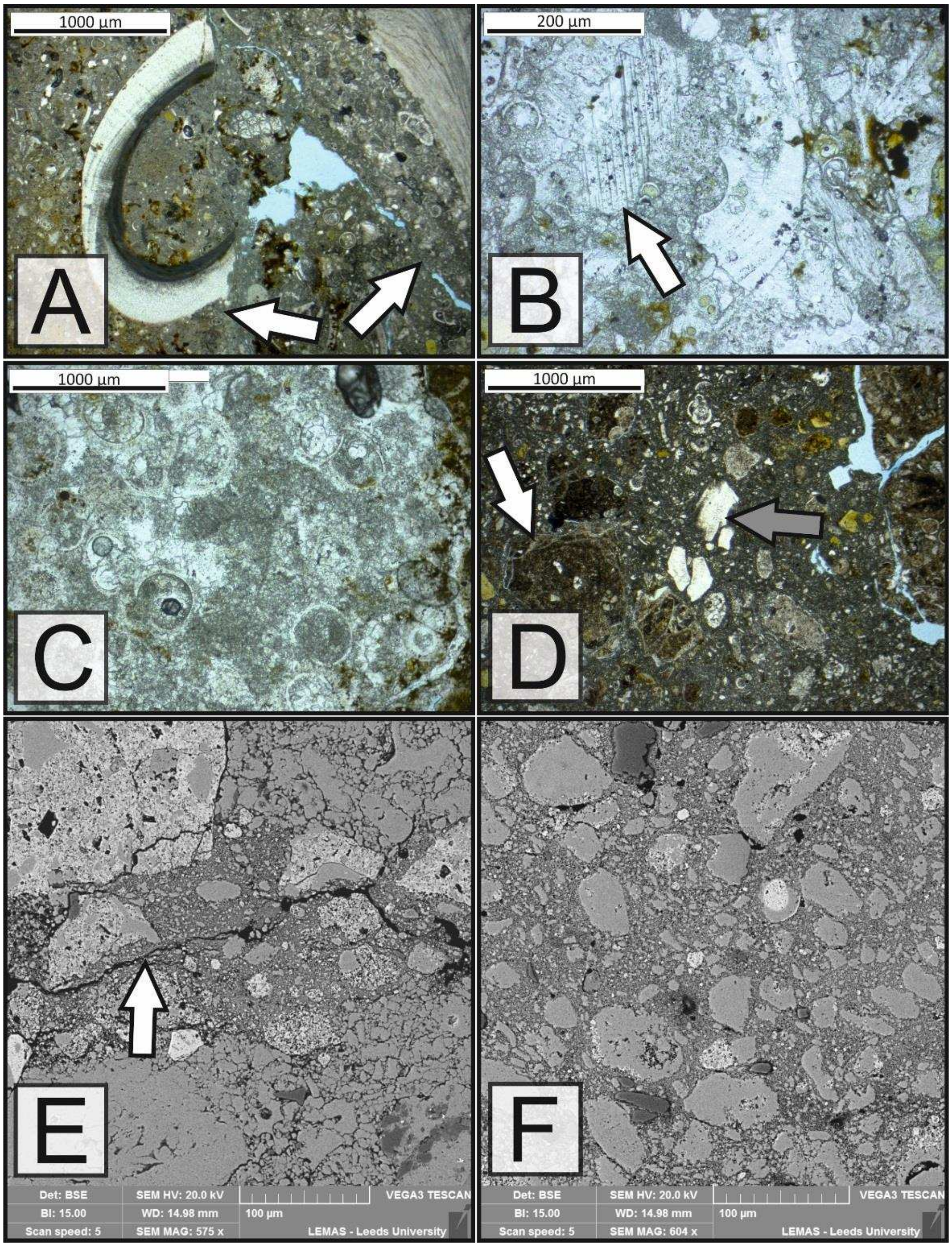

Figure 9: Polished optical photomicrographs (A-D) and BSE-SEM (E-F) images of fault rock from the micrite-dominated SQF slip surface. A) Fault breccia consisting of undeformed clasts surrounded by a finer grained fracture mesh. Arrows indicate clast – matrix boundaries, between which is finer grained, clay rich material. Clasts are often bound by open fractures, as indicated by the arrow to the right. B) Cemented fault rock exhibiting some calcite twinning (arrow). C) Undeformed LGL with calcite cements occluding inter- and

intra-granular cements. D) Breccia containing fractured phosphatised nodules (white arrow), skeletal fragments (grey arrow), and fine grained muddy matrix. E) BSE-SEM image showing open fractures (arrow) surrounded by fine grained material, including angular fragments of phosphatised nodules. F) BSE-SEM image showing cataclasis at the principal slip surface. Deformation of this kind is limited only to several millimetres of the slip surface. Globigerina grains resist cataclastic deformation, however other skeletal fragments are more prone to comminution and grain fracturing.

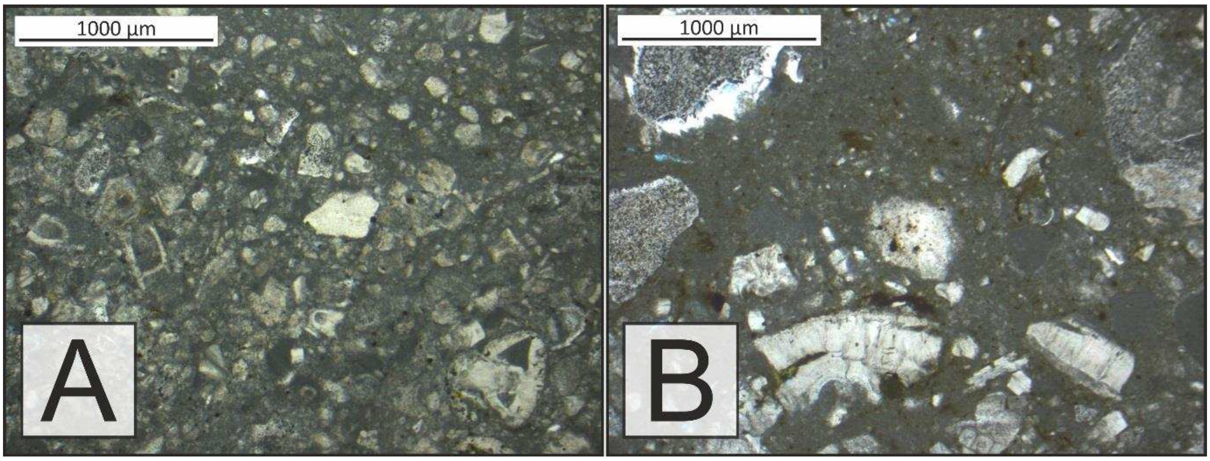

Figure 10: Polished optical photomicrograph images of fault rock from the grain-dominated LCL slip surface of the SQF. A) Grain scale deformation derived cataclasite immediately adjacent to the principal slip surface, consisting of grain fragments and micritic cements. B) Fracture derived cataclasite with fine grained matrix and clasts of bioclast fragments.

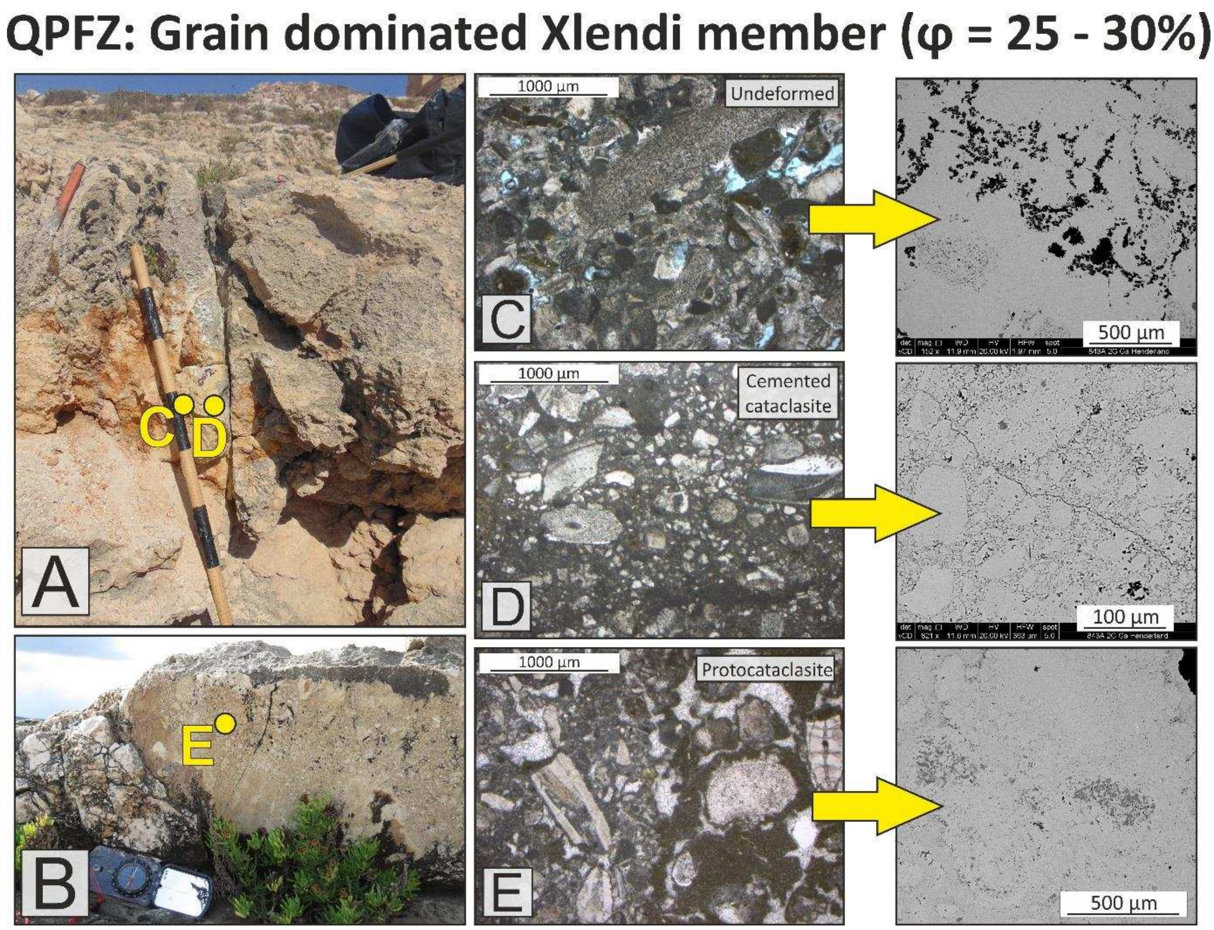

Figure 11: A) Southern bounding slip surface (unknown offset) of the QPFZ. B) Polished slip surface of the QPFZ principal slip surface. C) Xlendi member *c.*5 cm from southern bounding slip surface. D) Cemented cataclasite immediately adjacent to the southern bounding slip surface. Less rounded fossil clasts have become sub-rounded due to grain boundary dissolution and comminution. E) Protocataclasite from the principal slip surface with cemented matrix exhibiting 2 generations of cement (red micritic cement and later sparry calcite cement). Note the darker grey intragranular dolomite cements in the BSE-SEM image.

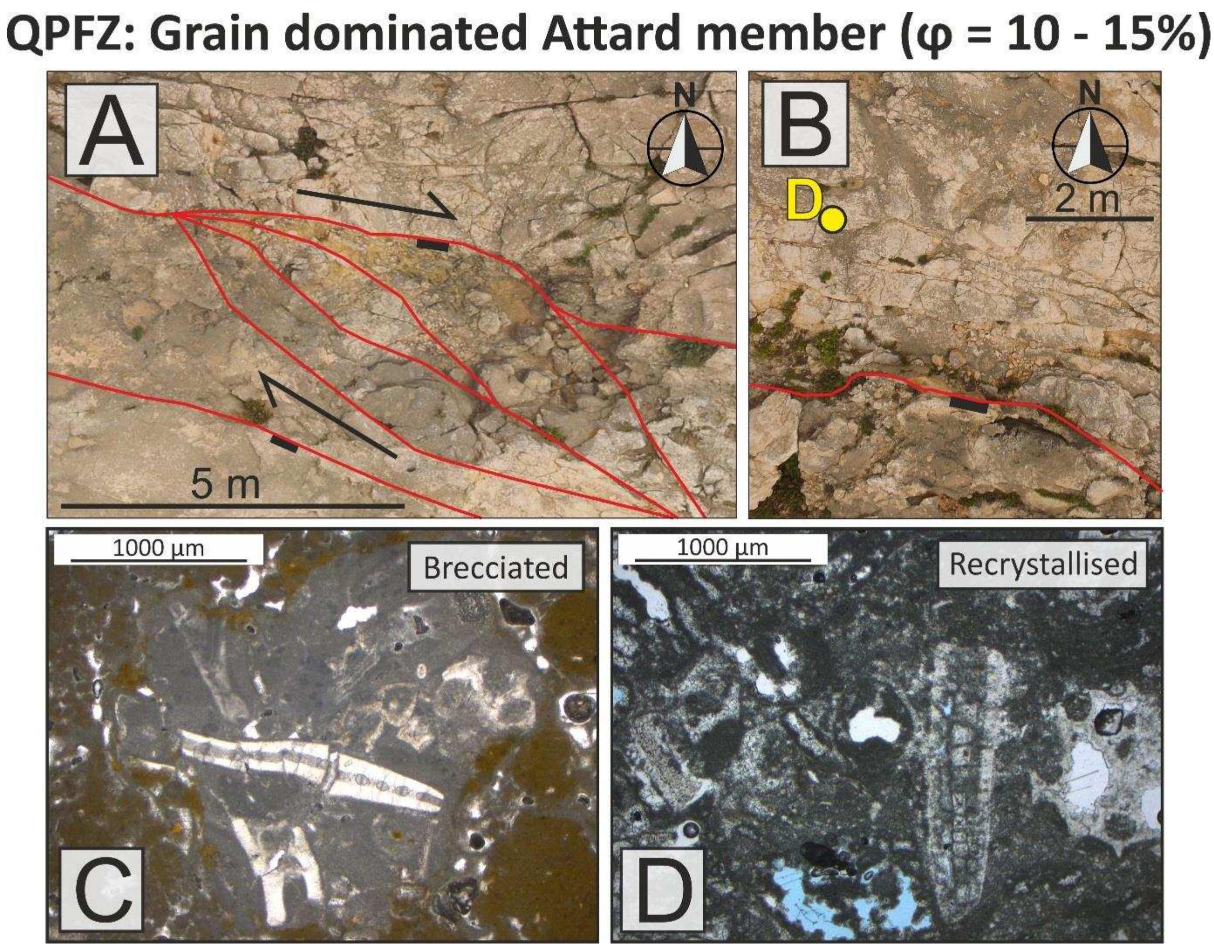

Figure 12: A) Releasing fault step over along the QPFZ principal slip surface indicating a dextral component to fault slip, with fault breccia. B) Anastomosing fractures/subsidiary slip surfaces in the QPFZ footwall, filled with a cemented and recrystallized core. C) Optical photomicrograph a clast of the Attard member within a Fe-rich cemented matrix. D) Recrystallized Attard member within FW fractures/subsidiary slip surfaces.

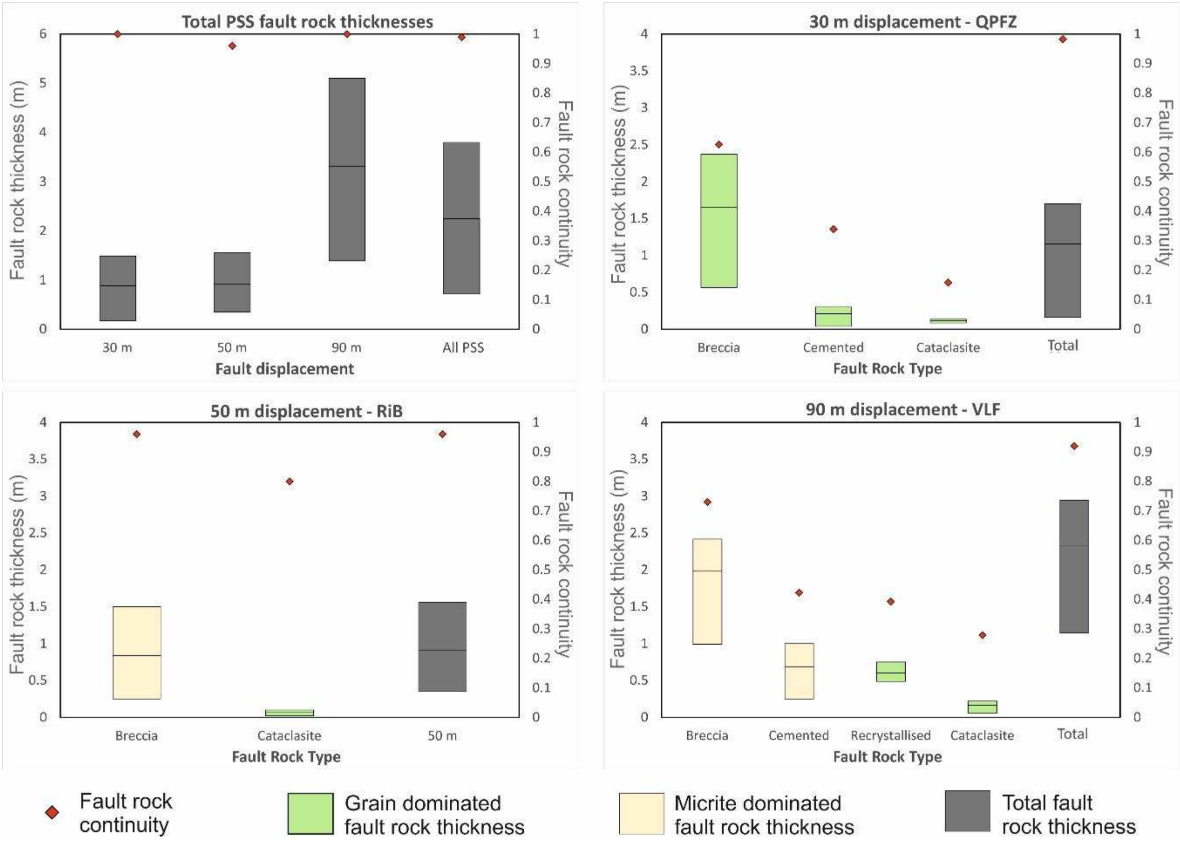

Figure 13: Plots of FRT and FRC measurements along fault strike for each fault rock type present at 3 Maltese fault zones. Box plots represent the interquartile range and arithmetic mean of fault rock thickness (FRT) measurements and are coloured according to lithology. Red data points represent the fault rock continuity (FRC). Top left: measurements of total fault rock thickness/continuity for each studied fault zone principal slip surface and all combined principal slip surface measurements. Other 3 plots show measurements of specific fault rock types at each specific fault zone, including along subsidiary slip surfaces (RIB = Ras il-Bajjada segment of the Il-Maghlaq Fault).

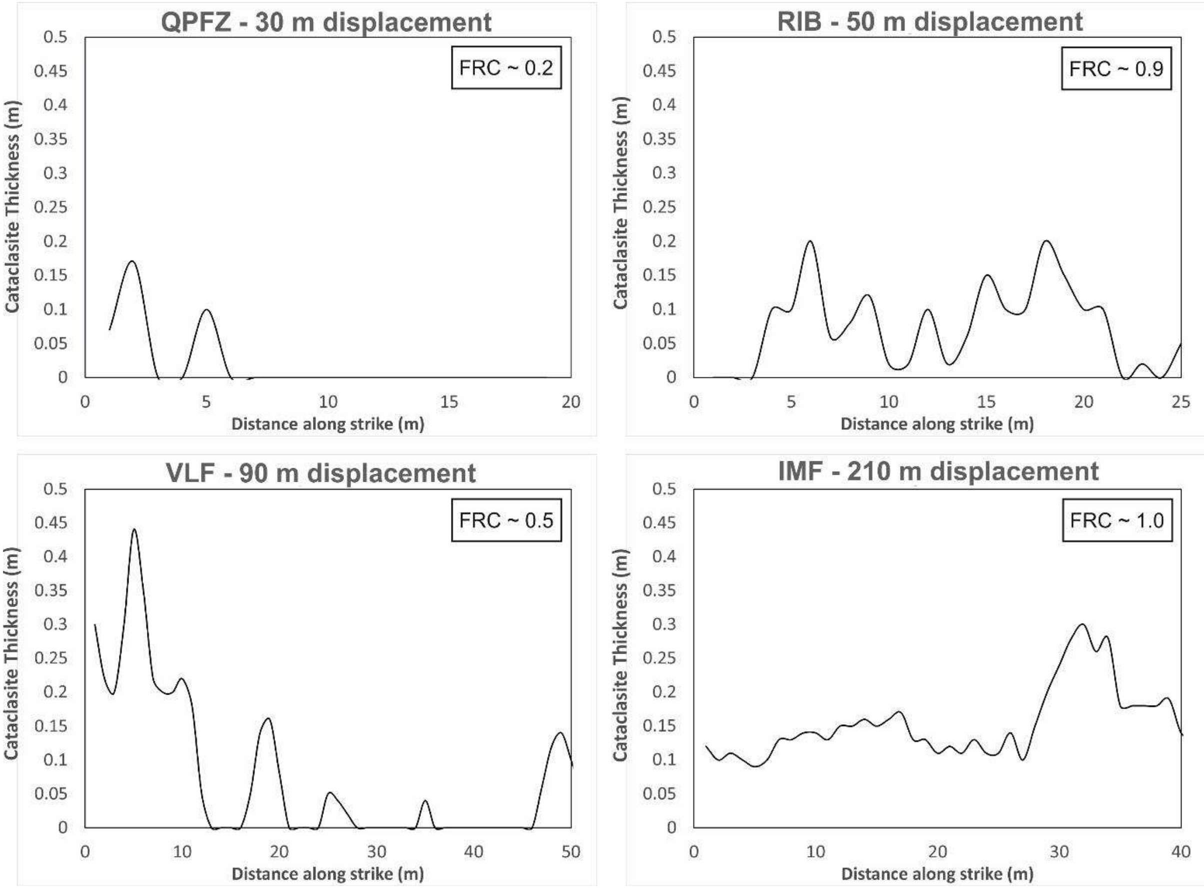

Figure 14: Cataclasite fault rock thickness within the grain-dominated LCL formation along strike of 4 fault zones. Clockwise from top left: Qala Point Fault Zone, Il-Maghlaq Fault (Ras il-Bajjada segment), Il-Maghlaq Fault, Victoria Lines Fault.

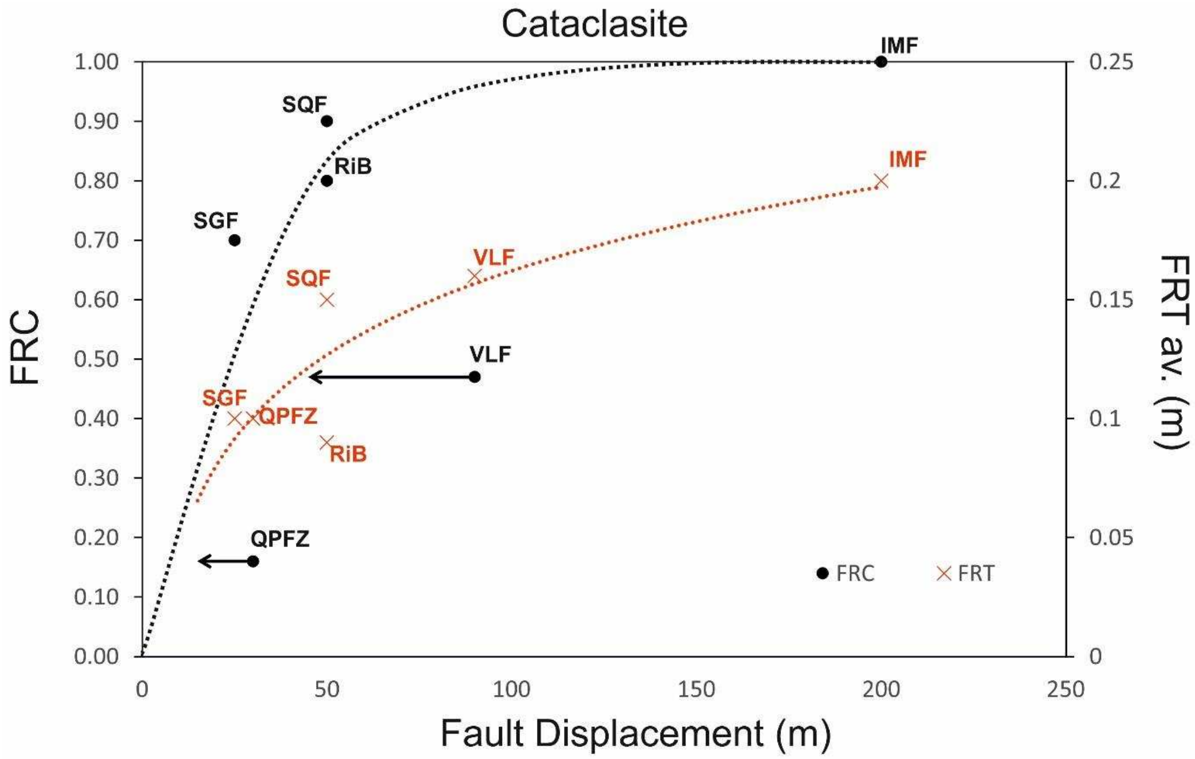

Figure 15: Estimated 2D fault rock continuity (FRC) and the arithmetically averaged fault rock thickness (FRT av.) for cataclastic fault rock, plotted against total fault displacement. Curves are hand drawn to highlight the data trend. All Maltese fault zones suitable for sufficient along strike thickness measurements are included. Black arrows highlight how the displacement across the principal slip surface is lower than the total fault zone displacement for fault zones with a distributed damage zone (QPFZ and VLF). Note that FRC values are a minimum estimate, as weathering may have removed some cataclasite exposure.

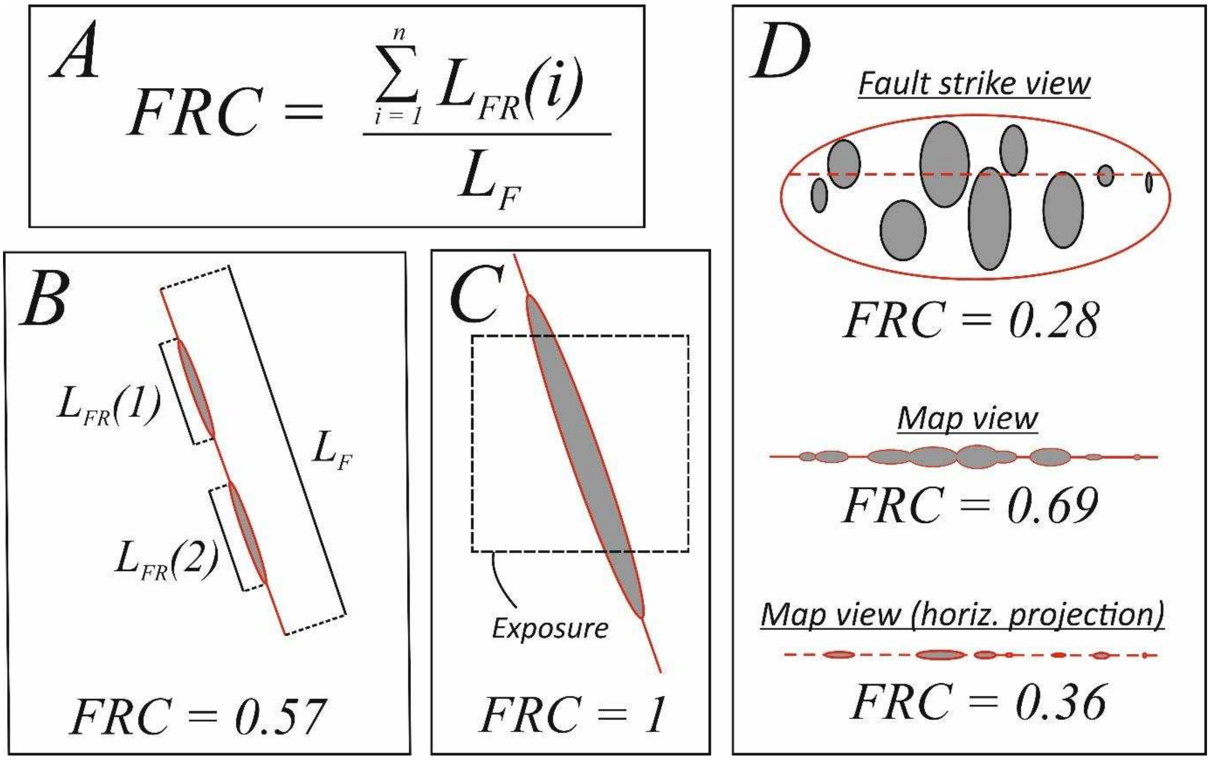

Figure 16: A) Equation used in calculating fault rock continuity (FRC). B) Example FRC calculation for a schematic map view of a fault zone with fault rock distributions (grey). C) Example of how a small exposure area relative to the size of fault distribution patterns can impact FRC calculations. Fault rock appears continuous (FRC = 1) from exposure, however the exposure does not account for the entire fault length, thus does not provide an accurate estimate of FRC. D) Schematic fault surface (observed from fault strike view) with a fault rock distribution. FRC is calculated for the entire fault surface based upon the area of fault rock coverage (0.28). Using the entire fault surface to calculate FRC in map view, based upon 2D length measurements, overestimates FRC (0.69). Projecting a horizontal plane across the fault surface (red dashed line) to simulate a map view exposure produces a more realistic FRC estimate (0.36).

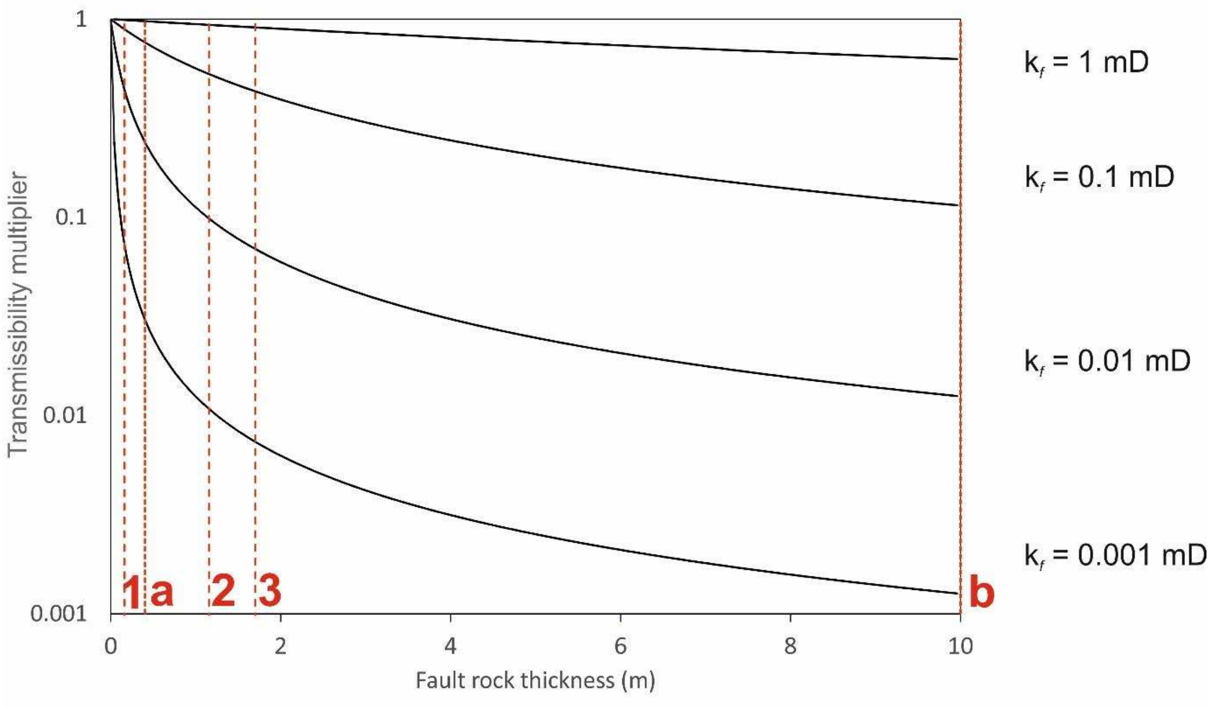

Figure 17: The impact of fault rock thickness on the calculated Transmissibility multiplier, for a range of fault permeability values (k_f). Host rock permeability values are taken from the 90 m displacement VLF: k_i = 2 mD, k_j = 200 mD (Michie et al., 2017). The dashed lines represent fault rock thickness values recorded from the VLF outcrop (lower quartile (1), arithmetic mean (2), and upper quartile (3)) and estimated fault core (a) and fault zone thickness (b) values for a 90 m displacement fault, extracted from empirical data presented by Solum & Huisman (2017).